INTERMEDIATE TEMPERATURE STRESS RUPTURE OF A WOVEN Hi-NICALON, BN-INTERPHASE, SiC MATRIX COMPOSITE IN AIR

Gregory N. Morscher
Case Western Reserve University, Cleveland, OH

Janet Hurst, and David Brewer
NASA Lewis Research Center, Cleveland, OH

ABSTRACT

Woven Hi-Nicalon™ reinforced melt-infiltrated SiC matrix composites were tested under tensile stress-rupture conditions in air at intermediate temperatures. A comprehensive examination of the damage state and the fiber properties at failure was performed. Modal acoustic emission analysis was used to monitor damage during the experiment. Extensive microscopy of the composite fracture surfaces and the individual fiber fracture surfaces was used to determine the mechanisms leading to ultimate failure. The rupture properties of these composites were significantly worse than expected compared to the fiber properties under similar conditions. This was due to the oxidation of the BN interphase. Oxidation occurred through the matrix cracks that intersected the surface or edge of a tensile bar. These oxidation reactions resulted in minor degradation to fiber strength and strong bonding of the fibers to one another at regions of near fiber-to-fiber contact. It was found that two regimes for rupture exist for this material: a high stress regime where rupture occurs at a fast rate and a low stress regime where rupture occurs at a slower rate. For the high stress regime, the matrix damage state consisted of through thickness cracks. The average fracture strength of fibers that were pulled-out (the final fibers to break before ultimate failure) was controlled by the slow-crack growth rupture criterion in the literature for individual Hi-Nicalon™ fibers. For the low stress regime, the matrix damage state consisted of microcracks which grew during the rupture test. The average fracture strength of fibers that were pulled-out in this regime was the same as the average fracture strength of individual fibers pulled out in as-produced composites tested at room temperature.

INTRODUCTION

The susceptibility of SiC fiber reinforced SiC matrix composites to strength degradation at intermediate temperatures (~ 500 to 1000°C) in oxidizing environments is well known [1-10]. The root cause of this "embrittlement" is due to the reaction of the oxidizing environment with the fiber-matrix interphase material.

For carbon interphase systems[1-4,6-8,10], the environmental reactions with the interphase forms a gap between the fiber and matrix which can be filled with SiO_2 reaction product as the fiber and matrix oxidize [11-13]. The stress-rupture

strength, σ_r, of these composites when the matrix is cracked [6] in an oxidizing environment is proportional to time with an exponent of ~ -¼ ($\sigma_r \alpha t^{-1/4}$) which would be expected if the critical flaw was controlled by passive oxidation layer growth on a SiC fiber[8,14]. With these time exponents, C interphase composites have been observed to have relatively short lives at intermediate temperatures once the matrix is cracked and the interphases separating the load-bearing fibers from the matrix have been removed.

It has been demonstrated that the stress-rupture properties of BN interphase systems (single tow CVI SiC minicomposites tested in tension [4,5] and CVI SiC matrix composites tested in flexure [9]) are superior to C-interphase systems due to the greater stability of BN in oxidizing environments. The time exponents determined for single tow minicomposites tested at 700 and 950°C in air range from - 0.025 to - 0.038, respectively [4,5]. This order of magnitude reduction in time exponent would result in hundreds or even thousands of hours improvement in lifetimes for stresses above the matrix cracking stress of SiC/SiC composites compared to composites with a carbon interphase.

For these systems, a relatively short (microns) distance of interphase is recessed, compared to C (millimeters). BN reacts with O_2 and H_2O in the environment due to the formation of gaseous (H-B-O containing gasses) and condensed phase oxidation products (B_2O_3 liquid or borosilicate liquids or glasses) [15-16]. Yet, this recession and reaction product formation still cause fiber degradation [4] and/or fiber-matrix bonding resulting in local stress concentrators [17] on the fibers in the region of the matrix crack.

In this study, the intermediate temperature rupture properties of BN-interphase SiC/SiC composites will be extended to a melt-infiltrated (MI) matrix composite. Melt-infiltrated composites are much denser than CVI-matrix composites and as a result have higher matrix cracking stresses than CVI-SiC matrix composites [18]. The tensile stress rupture properties of a woven Hi-Nicalon™ fiber, BN interphase, melt-infiltrated SiC matrix composite was determined at intermediate temperatures in air. Some rupture data for this composite system has been taken by Brewer et al. [19] who have tested this material under low-cycle fatigue (LCF) conditions (2 hour hold stress followed by an unload-reload cycle) at 815°C in air. Similar stress conditions will be applied in this study under constant stress. This will be done in order to determine if any effect of load-cycling further degrades the lifetime of these composites which was found to be the case for single tow minicomposites [5].

An important consideration for understanding composite lifetime will be the matrix damage state for the given applied stress. Damage accumulation for this Hi-Nicalon/BN/MI SiC woven composite system [18] occurs over a range of stress. The onset of microcrack formation in the large matrix regions and 90° bundles (tows) occurs at a low stress (~ 75 MPa). As stress is increased, microcracks grow and/or new cracks are formed that intersect load-bearing bundles which eventually results in the formation of through-thickness cracks with increasing stress. The damage accumulation for this material system was fairly well quantified with modal acoustic

emission (AE) monitoring coupled with unload-reload tensile hysteresis experiments at room temperature [18]. In this study, AE monitoring similar to that performed for the room temperature experiments will be performed during the stress-rupture experiments in order to locate and quantify the extent of damage.

EXPERIMENTAL

Material Properties

Several properties of the composite constituents are described in Table I. The material consists of eight plies of woven 17 ends-per-inch Hi-Nicalon, a ~ 0.5 μm boron nitride interphase, and a melt infiltrated (MI) SiC matrix. The matrix was processed in several steps. First a thin (~ 2 μm) layer of SiC was applied by chemical vapor infiltration to the BN coated woven preform. A SiC particle containing slurry was infiltrated into the porous network. This was followed by infiltration of molten silicon that nearly filled the porous network. Therefore the matrix is predominantly SiC with some Si.

Mechanical Testing

The tensile test set-up is shown in Figure 1. Most tensile tests were performed using a screw-driven universal testing machine*. One test was performed on a hydraulic universal testing machine#. The test specimen dimensions were 2.1 mm thickness, 12.5 mm width and 150 mm length. Graphite-epoxy tabs (0.08" thick) were glued to the ends of the bars. The test specimens were gripped with hydraulic grips in the tabbed region. Wide band (50 kHz to 2 MHz) acoustic emission sensors** were attached to the ends of the tensile specimens within the grips with quick setting epoxy. This was done to insure that the temperature the sensors experienced was maintained at approximately 25°C. A resistance-heated furnace ($MoSi_2$ elements) was used to heat the center section of the specimens. The furnace dimension in the tensile direction was 75 mm; however, the hot zone was only approximately 15 mm.

AE monitoring was performed with a Digital Wave Fracture Wave Detector**. The AE set-up and wave-form analysis is given in greater detail in reference [21]. It is important to note that the location of the events could be determined from the speed of sound of the damaged material, which was determined experimentally, and the difference in times of arrival of the waveforms corresponding to the same event on the two AE sensors.

The experimental test procedure was as follows:

1. Samples were mounted in the machine and pencil lead breaks were performed at an edge and on the face at a known distance from one of

---

* Instron 4502, Instron, Canton, MA.

Instron 8500????, For this test, an induction heated SiC element furnace was used.

** Digital Wave Corp., Englewood, CO

the edges in order to determine the speed of sound in the undamaged state.

2. The furnace was heated up to the desired set temperature. Acoustic emission was monitored at the beginning of the heating cycle and was continued until the final failure of the material. A constant tensile load of 100 N (3.8 MPa) was applied under load control during heating to account for the thermal expansion of the material
3. SiC contact extensometers were applied to the edge of the tensile bar.
4. The sample was loaded to the predetermined tensile load at 0.25 mm/min. The sample was then held at the predetermined load until failure.

Matrix Cracking Determination

In order to determine the damage accumulation, several of the ruptured composites were cut and polished along the length of the tensile bar using standard metallographic techniques. Composite lengths of ~ 40 mm on one side or the other of the fracture surface were mounted and polished. These polished portions included the length of composite exposed to the hot zone region as well as regions exposed to lower temperatures. The polished samples were plasma etched with HF in order to enhance the matrix cracks.

Plasma etching would severely etch the Si in the MI matrix which made it difficult to observe cracks which were through several plies or through the thickness of the composite. The cracks through the CVI SiC surrounding the tows were easily observed. Therefore, the crack spacing in the CVI SiC was determined for an interior ply and an exterior ply. For the three composites observed, the difference in the number of cracks between the two plies was less than 10%. The crack spacing was determined over ~ 10 mm lengths of the tensile bar.

Scanning Electron Microscopy

The fracture surfaces were examined with a conventional[#] (SEM) and/or field emission[##] (FESEM) scanning electron microscope. For the FESEM, a voltage of 5 kV was used which required no conductive coating. General observations were made on the fracture surfaces. Individual fiber fracture surfaces were also obtained from various regions of the fracture surface in order to perform fiber fractography analysis. Electron dispersive spectroscopy (EDS)[###] was performed on matrix, interphase, and fiber surfaces to determine the extent of oxidation. Microscopy was performed on samples tested in this study as well as on two fracture surfaces of specimens that were obtained from Brewer et al.[19]

[#] Jeol JSM 840A, Tokyo, Japan

[##] Hitachi S4500, Tokyo, Japan

[###] Kevex 4460 Pulse Processor with Quantum Ultrathin Window and IXRF Systems, Inc. Software.

RESULTS AND ANALYSIS

Mechanical Data

The stress-rupture results versus time are shown in Figure 2. The experiments were performed with a furnace hot zone temperature thought to be 815°C in order to compare this data with the data of Brewer et al. [19]. The first two specimens failed outside of the hot zone. Therefore, the furnace profile was determined with a thermocouple that was translated through the furnace at 1 mm increments. The hot zone temperature for the conditions of the first two experiments was found to be 960°C (Figure 3). The temperature where the first two rupture specimens failed was ~ 880°C. The hot zone temperature for the next four rupture specimens was truly at 815°C. Two of those samples failed in the hot zone and two of those samples did not fail for the allotted time of the experiment (138 hours).

The 815°C fast fracture strength is also plotted on Figure 2 [19]. Combining the two sets of data, there appears to be two rupture regimes: a more severe rate of rupture occurs at higher stresses whereas a less severe rate of rupture occurs at lower stresses. There is a slight difference in the transition stress between these two regimes for the two sets of data. The data from Brewer et al. having better rupture properties and a higher transition stress (~ 165 MPa) compared to the material tested in this study which had a transition stress of ~ 150 MPa. The high stress regime will be referred to as Regime I and the low stress regime will be referred to as Regime II. For the sake of comparison, the time exponent for Regime I is ~ -0.13 and the time exponent for Regime II is ~ -0.02.

The stress-strain curves for several stress-rupture experiments and for a room temperature fast fracture test of a specimen from the same panel are shown in Figure 4. The initial loading of the stress-rupture experiment is identical to that of the room temperature stress-strain curve up to the rupture stress after which additional strain is accumulated with time. Note that the transition stress between the two rupture regimes is at the beginning of the "knee" in the stress-strain curve.

The "knee" is associated with increased damage in the matrix in the form of through thickness cracking. The room temperature stress-strain behavior obtained for the ref. 18 material and the room temperature stress strain behavior of the samples tested in this study are plotted together with the intermediate rupture behavior in Figure 5. The room temperature stress-strain curves are very similar except that the "knee" in the curve occurs at a lower stress for the material tested in this study compared to the material tested by Brewer et al.[19]. In fact for both materials, the transition stress corresponds to the beginning of the "knee" in the stress-strain curve, i.e. through thickness cracking. Therefore, the higher stress rupture rate appears to occur for a matrix state of through thickness cracking; whereas the low stress rupture rate appears to occur for a matrix damage state of non-through thickness microcracks.

Because of this correlation, an additional experiment was performed where the composite was precracked at 230 MPa at room temperature and tested at 815C

at 110 MPa (Figure 2). It was thought that this rupture condition could result in a failure time corresponding to the rupture rate for Regime I (~ 30 hours). However, the specimen lasted much longer than expected and after 138 hours the experiment was stopped.

Acoustic Emission Data and Matrix Crack Spacing

Modal AE was used to monitor the damage occurring along the length of the rupture specimens during the experiment. Two examples are shown in Figure 6 of the AE source locations plotted versus time for an experiment performed at 960°C and one performed at 815°C. The location was determined by the difference in times of arrival of the initial extensional wave portion of the AE waveform based on the accumulated damage (reduction in elastic modulus) [20-21]. The data was sorted so that only events which occurred in the $\pm$ 30 mm region of the sample were analyzed. The data was also sorted according to the energy of each AE event. The events with the two highest decades of AE energy are plotted separately and the events with the three lowest decades of AE energy are combined in Figures 6a and 6b. The loads plotted in Figures 6a and 6b are the loads recorded by the AE computer when an event occurs. The apparent load fluctuations are not real but are the result of signal noise from the universal testing machine received by the AE computer through the analog input*.

Several details are worth noting from the AE studies. For example, Figure 7 shows the cumulative number of events and cumulative AE energy from each event versus time for three different rupture experiments. For the lowest stress (Regime II) specimen, most of the AE events and the AE energy occurred after reaching the rupture load. For the highest stress (Regime I) specimen, most of the events and most of the AE energy occurred during loading. For the middle stress specimen (Regime I), most of the events occurred after loading whereas most of the energy occurred during loading. It has been shown in other studies that matrix cracking correlates well with the largest energy events [18,21] and not necessarily the number of events. Therefore, Regime I material was fairly well cracked prior to the set-load and some additional cracking occurred afterward; whereas most of the cracking occurring in the Regime II material occurred after the set-load was reached.

Second, the failure location# was accurately predicted from the location analysis (final AE event) for both specimens as shown in Figure 6. In fact, the

---

* The AE computer was connected to the Instron through the connector for analog output. The load output that was conditioned, digitized, and received on a different computer showed no load fluctuations (see Figure 4). Therefore, an oscilloscope was tied into the same output from the Instron to the AE computer. It was found that a periodic, low frequency noise always occurred even when no load was applied. The peak amplitudes of this low frequency noise corresponded to the largest load fluctuations plotted in Figures 6a and 6b. This noise had no effect on the AE signals, which were received through different channels.

It was determined that the amount of AE activity on loading was the same as occurs for room temperature tensile loading [18,20]. The AE activity for these low stress/strain conditions primarily corresponds to matrix cracking. Therefore, the initial damage state at the start of the rupture experiment can be considered the same as the damage state of the same composite for the same

location of all four rupture specimens determined by the AE method were within ± 1 mm of the actual measured location. This confirms the accuracy of the AE source locations as pertaining to real physical phenomena. It is also clear that there were a number of high energy events for both specimens occurring at approximately the same location as the final failure event prior to the failure time. These high energy AE events must have been caused by the formation of large cracks or the growth of existing cracks at that location.

Third, the location of damage is apparently temperature dependent based on the AE activity as a function of location, i.e. temperature profile. In Figure 6a, AE activity is significantly less in the hot zone (960°C) region after ~ 1000 seconds compared to the regions just outside the hot zone. Conversely, in Figure 6b, more AE activity occurs in the hot zone (815°C) region.

The crack spacing was determined for several ruptured composites. Figure 8 shows the temperature dependence of crack spacing as a function of length of two specimens tested at 960°C. It is evident that more cracking occurred in the 700 to 900°C exposed region of the composites than at regions exposed to higher or lower temperatures. The lower stress condition resulted in twice as many cracks in this region compared to the hot zone temperature region whereas the higher stress condition resulted in 50% more cracks in the 700 to 900°C exposed region compared to the hot zone exposed region. For a specimen tested at 815°C, most matrix cracking occurred in the hot zone region (Figure 9). The matrix crack spacing was also shown in reference 20 to correlate well with the cumulated AE energy along the length of the specimen.

For both specimens in Figure 8 there was considerable AE activity in the ± 25 to 30 mm regions of the samples. There is also considerable activity beyond these distances which had been removed from the data sets for the plots shown in Figure 6. This is especially pronounced for the longer time experiment (Figure 6b). A cumulative energy analysis and crack spacing measurements were made on both samples [22]. For these regions, there was very little increase in the AE energy after the set-load was reached. Also, the matrix crack spacing in these regions was less than the matrix cracking closer to the gage section of the composite. When compared to other tests performed at room temperature, it was concluded that this noise corresponded to microcracking associated with the bending stresses applied to the tensile bar fairly close to the grips and not due to any temperature/environment effect [22].

Microscopy of Composite Fracture Surfaces

Two representative fracture surfaces are shown in Figures 10 and 11 from Regimes I and II, respectively. The fracture surface of the Regime I tested specimen

---

stress-strain condition at room temperature. The speed of sound decreases with the square root of modulus as damage in the matrix is accumulated [21]. The speed of sound used in the location analysis was based on the known speed of sound for the room temperature tested composite at the same starting damage state [18] for each rupture starting condition.

(Figure 10) is characterized by a "picture frame" type of appearance [14]. The outer layer of tows on the face and edges of the cross-section have little or no pull out whereas the interior fibers have all pulled out. The outer embrittled tows still have BN surrounding most of the fiber except where fibers are in near contact to one another (Figure 10b). The oxidation reactions occur first at the fiber/BN interphase probably enhanced by the presence of a thin carbon layer on the fiber surface resulting from the high temperature MI process temperature [23,24]. Since fibers are separated by only a fraction of a micrometer, the larger BN surface area exposed to the environment in these near contact regions results in a greater amount of BN volatilization and oxide formation [16]. Nearly every fiber fracture mirror is observed to emanate from these near fiber contact regions (Figure 10b). A similar observation was made for Hi-Nicalon/BN/CVI SiC minicomposites tested at slightly higher temperatures (900 to 1050°C) [4-5] where fracture mirrors emanated from fiber-matrix bonds formed by the solidified oxidation product. For the fracture surface shown in Figure 10a, approximately ten tows were embrittled which corresponds to ~ 19 % of the load-bearing tows. For another sample tested at 165 MPa and a rupture time of 2.8 hours with the same type of picture frame appearance, eighteen tows were embrittled corresponding to ~ 34 % of the load-bearing tows.

There was little evidence of oxidation at near fiber contact regions for the interior fibers that pullout under regime I conditions. The transition from embrittled fibers to pulled-out fibers represents the oxidation reaction front in the through-thickness crack for the short time rupture specimens. The oxidation front is presumably controlled by the kinetics of O_2 and H_2O ingress and consumption when reacting with the BN and SiC.

The fracture surface for the low stress regime tested specimens (Figure 11) is characterized by a more jagged appearance. First, the fracture takes place on several different crack surface "planes" sometimes separated by up to 3 mm in the loading direction. Second, instead of forming a picture frame, it appears these smaller local cracks grew into the interior of the sample so that some interior bundles are embrittled while some surface bundles have fiber pull out. Figure 11b shows a fairly sharp transition in a single tow separating the embrittled fibers from the apparently pristine fibers. Figure 11c also shows a typical oxidized crack surface where borosilicate liquid/glass had formed to fill the interphase regions surrounding the fibers and the crack surfaces.

EDS Analysis

EDS was performed on individual fiber fracture surfaces from two composite fracture surfaces, one from Regime I and one from Regime II. The Regime II composite fracture surface and EDS analysis are shown in Figure 12. EDS was performed on several fibers from seventeen different fiber bundles on the fracture surface. The O:C ratio peak height ratio from the EDS spectrum was calculated (Figure 12c). The data was organized according to the O:C peak height ratio and a map of the fracture was constructed based on relative O:C ratios. (Figure 12b).

The pulled out fibers had the lowest O:C ratios which would be expected if the final failure event consisted of pulled-out fiber failure. For the embrittled fiber bundles only one corner of the composite cross-section showed high O:C ratios indicative a relatively thick SiO_2 scale and early fiber failure. The rest of the embrittled bundles showed higher O:C ratios than the pulled-out fibers, although not significantly higher. There does seem to be a consistent lowering of O:C ratio for the fiber bundles closer to the pulled out bundles. An arbitrary distinction is made in Figure 12b for regions of $1.5 < O:C < 2$ and $1 < O:C < 1.5$. The O:C ratio of the matrix surface around all of the embrittled bundles was on the order of 4 to 10 with the exception of a few regions where parts of a bundle appeared to be "sealed" by the oxidation product.

EDS analysis was performed on the fracture surface shown in Figure 10 (Regime 1). The time to failure for this specimen was only one hour. The O:C ratio for pulled out fibers was $\sim 0.25 \pm 0.01$ from three different bundles. The O:C ratio for embrittled fiber fracture surfaces ranged from 0.24 to 0.41 from seven different bundles. The O:C ratio for the matrix regions in and around the embrittled bundles ranged from 0.5 to 0.8. As with the Regime II fracture surface, the pulled-out fibers had lower O:C ratios indicating they failed last. Also, there was only a small difference in O:C ratios between the pulled-out and embrittled fibers.

Therefore, it can be concluded that embrittled fiber failure occurred prior to pulled-out fiber failure. However, the time period between most embrittled fiber failure and pulled-out fiber failure was fairly short. The embrittled fibers must have been bridging the matrix cracks for considerable periods of time before failing. When the embrittled fibers did fail, the load they were carrying was shed onto the remaining fibers. In order to determine the criterion for fiber failure in the different regions of the composite fracture surface, fiber fractography was employed.

Fiber Fractography

The fracture mirrors of individual fibers were used to determine the relative (average) strengths of fibers on the ruptured composite fracture surfaces. Three groups of fracture surfaces were observed for each sample evaluated: embrittled fibers, pulled out fibers in the 2nd ply from the surface and pulled out fibers in the 4th ply from the surface (middle ply). Also, the fracture mirrors were determined for one of the room temperature tested tensile specimens.

The strength of the fibers, σ_f, is related to the mirror radius, r_c, by the relationship:

$$\sigma_f = A r_c^{-1/2} \qquad (1)$$

where A is the fracture mirror constant. The data was to be compared on a relative stress basis, i.e. the tensile rupture stress divided by the room temperature ultimate tensile stress. For this reason, only the mirror radius needs to be determined. The

normalized rupture stress from fracture mirrors was determined from the relationship:

$$\sigma_{fm(T,t)}/\sigma_{fm(RT)} = \{\underline{r}_{c(R.T.)}/\underline{r}_{c(T,t)}\}^{1/2} \qquad (2)$$

where $\underline{r}_c$ is the radius corresponding to a 63.2% probability to failure (when ln[ln(1/1-P)] = 0 where P = probability to failure), (T,t) refers to the rupture condition, and (R.T.) refers to room temperature. At least forty fibers were used for each distribution.

The results for four different fracture surfaces are shown in Figures 13 and 14 for two Regime I and two Regime II specimens, respectively. For all of the samples observed, the pulled out fibers showed the same strength properties regardless of the ply, so they will be grouped together.

For both sets of data, the embrittled fibers fail at approximately 70 to 80% of the room temperature ultimate strength. However, there is a dramatic difference in the failure strength of the pulled-out fibers between the two different rupture regimes. Pulled out fibers for Regime I composites fail at an even lower stress (~ 65% of the room temperature strength) than the embrittled fibers. Pulled out fibers for Regime II composites fail at approximately the same strength as the room temperature failed fibers. It is evident that *a different failure criterion for the pulled-out fibers controls their failure for the two regimes.*

To understand these strength levels, also plotted in Figures 13 and 14 are the normalized average fiber stresses corresponding to the applied rupture load. These include the applied stress, the stress on the pulled-out fibers if the embrittled fibers failed first (load-shed stress), and the rupture stress condition for individual as-produced Hi-Nicalon fibers at the same time-temperature condition [25]. To determine the load-shed to the pulled-out fibers, the number of tows that were embrittled on the composite fracture surface was estimated as explained above and the load those tows would have carried was added to the applied load of the pulled-out tows. The rupture stress condition for individual as-produced fibers as determined by Yun and DiCarlo [25] is shown in Figure 15 as a Larson-Miller plot. The time, temperature regime is highlighted which corresponds to this study and is referred as the "L-M Condition" on Figures 13 and 14.

Several observations can be made from comparing these stress conditions with the actual measured fiber strengths:

1. The failure stress of all the composites (applied stress) was significantly lower than the expected rupture stress for Hi-Nicalon fibers if the fibers were carrying all of the load in the matrix crack (L-M Condition).
2. The embrittled fibers appear to fail at stresses slightly higher than the as-produced fiber rupture criterion (L-M Condition).
3. For Regime I, after the load is shed onto the pulled-out fibers, the load-shead stress is about equal to the Hi-Nicalon L-M Condition stress. Both stresses are in good agreement with the measured (fiber fracture mirrors) normalized strength of the pulled-out fibers for Regime I materials.

4. For Regime II, after the load is shed on the pulled-out fibers, the load-shed stress is much higher than the Hi-Nicalon L-M Condition criterion, even approaching the ultimate strength of as-produced fibers. This load-shed stress is in good agreement with the measured (fiber fracture mirrors) normalized strength of the pulled-out fibers for Regime II material.

Two conclusions can be drawn from these observations. First, since the embrittled fibers fail first, their apparent "strength" is due to the local bonding of the fibers to one another because of the oxidation product formation. Similar to the minicomposite results [4], the fibers are probably weakened slightly by the stress-condition and oxidation reactions; however, they are also strongly bonded to one another resulting in shorter gage lengths and local stress-concentrations. As with minicomposites [4], a weak fiber fails after some time at temperature. The load from this fiber is shed locally [26] rather than globally due to the interphase condition resulting in the progressive and probably rapid failure of bonded fibers.

Figure 10b shows a group of fibers where each fiber is in close contact (less than 100 nm) to at least one other fiber. The close contact is due to the tightness achieved during the weaving operation and pressure applied to the weave, to maintain dimensional stability of the panel during CVI BN infiltration [27]. In order to quantify the extent of fiber-to-fiber contact an as-produced composite was polished and the groupings of fibers were determined for individual tows from a surface ply, the second ply from the surface, and the center ply (fourth ply from the surface). The results are given in Table II.

A group was defined as the number of fibers that were in close contact to at least one other fiber from the same group. The groups are categorized according to a single-fiber (no-touch) group, two-fiber group, three-fiber group, less than 10-fiber group, and less than 20-fiber group. There are few fibers from a 500 fiber count bundle that are in groups of only a few fibers. In fact, about two-thirds of a surface tow have fibers in groups of 20 or more. Groups containing 20 or more fibers are even more prevalent for bundles located in the interior of the composite.

If fiber failure (in the embrittled regions) is correlated with the failure of a low-strength neighboring fiber, then large portions of a load-bearing tow, if not the entire tow, could fail immediately after the failure of the single fiber in a large group of fibers. This nearly instantaneous, progressive failure could also be extended to neigboring tows in the same microcrack.

This process is controlled mostly by BN oxidation at the near fiber-to-fiber contact regions and the small amount of condensed phase oxidation product required to form a bond between two nearly contacting fibers. If more uniform ($\sim$ 0.5 μm) BN layers could be applied without the near fiber-to-fiber regions, this process is expected to be slowed down. Minimal fiber-to-fiber or fiber-to-matrix contacts, because of more uniformly coated fibers, is probably why the rupture properties of minicomposites are superior to macrocomposite rupture properties at intermediate temperatures. More uniform interphases could possibly be achieved

by weaving already coated fibers within tows or by using processing approaches that enable greater separation of fibers.

Second, for Regime I conditions, the fibers which have not been exposed to the environment are still being loaded and are weakening according to the intrinsic degradation mechanisms operating at the stress/temperature/time conditions [25] since the matrix cracks are through-thickness. For Regime II conditions, microcracks must grow into the material in order for new fiber bundles to be exposed to the environment and for the fibers to be fully loaded. The loading of the fibers in the uncracked regions, where fibers have not been exposed to the environment, should be a fraction ($\sim$ 1/3 based on the rule of mixtures) of the loads applied to fully loaded fibers bridging a matrix crack since the matrix is sharing the load.

Room Temperature Strength of Rupture Specimens Which Had Not Failed

Two composite specimens did not fail after 138 hours at 815°C. One had been precracked at 230 MPa and held at constant stress of 115 MPa. The other specimen was loaded to and held at 130 MPa for the duration of the experiment. Both of these specimens were tested in tension to failure at room temperature. The precracked specimen failed at 109 MPa just outside the hot zone region. The non-precracked specimen failed at 81 MPa in the hot zone region of the specimen. Both specimens failed at lower stresses than the applied rupture stress. There was very little non-linear stress-strain behavior or acoustic emission activity for either specimen.

For the *non-precracked specimen*, there was little fiber pullout on the fracture surface (Figure 16a). Ironically, the only fiber pullout existed at eight of the bundles near the surfaces of the specimen. Almost all of the embrittled bundles only showed minor amounts of oxidation (Figure 16b) which always occurred at the fiber-to-fiber contact points. The BN around the rest of the fiber was almost always present except for a few bundles near the surface of the composite.

From EDS analysis, the matrix failure crack surface contained no oxygen, indicating that most of the failure crack did not propagate along an existing matrix crack. This occurred, even though fiber-bridged cracks were observed (after the experiment) to have traversed through half of the composite thickness during the rupture experiment. Two matrix fracture surface locations were oxidized within fiber bundles. One region near an edge and the other near a face surface. It is apparent that the failure crack started at an existing crack but propagated in a relatively planar fashion (compared to rupture fracture surfaces) through previously uncracked but embrittled fiber bundles.

The fiber-bundle embritllement came from oxidation along the length of the fibers at the fiber/BN interface where a thin carbon layer resides as a result of fiber decomposition from matrix processing [23,24]. This pervasive oxidation is most prevalent at the near fiber-to-fiber contact regions (Figure 16b) because of the increased surface area for BN oxidation after the initial oxidation of carbon [24].

However, a thin oxide layer was observed to exist in between the fiber and the BN where the fibers were not in contact (Figure 16c) throughout the fracture surface.

Ogbuji[24] observed this kind of "pervasive" oxidation for uncracked specimens subjected to a burner rig conditions (800°C, 10% H2O, 105 m/sec, 1 atm). Ogbuji also showed that for specimens exposed to lower and higher water vapor contents in a tube furnace little if any "pervasive" oxidation occurred. For burner rig conditions, oxidation of the 0° bundles occurred through the exposed 90° bundles. For the case of this study, it is believed that the 0° oxidation occurs through the exposed 0° fibers at a matrix crack some distance away from the failure crack at room temperature.

For the *precracked specimen* very similar features were observed except that no fiber pull-out was observed and that most of the matrix was oxidized, i.e the failure crack propagated along an existing matrix crack. The region where failure occurred corresponded to an exposure temperature of ~ 770°C. Still, most of the BN was present around a fiber and all of the fiber-to-fiber contact locations were oxidized and were the source for fiber fracture mirrors.

DISCUSSION

The rupture and residual strength properties of these composites are obviously controlled by the reactions of the fiber/matrix interphase with the environment and the prevalence of near fiber-to-fiber contacts. However, for Regime I conditions, the embrittlement is caused by the ingress of the oxidizing gasses into an already existing through-thickness crack. For Regime II conditions, embrittlement is caused by microcrack slow-crack growth as a result of embrittlement of the fibers exposed to the environment and is thus slower than Regime I behavior. This also explains why a greater amount of cracking is detected by AE for Regime II composites than Regime I composites during the constant load portion of the experiment.

The differences in rupture properties between the two different batches of material tested in this study and in ref. 19 can be related to slightly different damage states at the same stresses. Surprisingly, there does not appear to be any difference due to the constant load conditions of this study and the LCF conditions of ref. 19. Minicomposite data showed a significant difference between these two stress states at slightly higher temperatures (900 to 1000°C) [5]. That is, the time to failure for minicomposites tested under constant load conditions was orders of magnitude greater than when tested under low frequency fatigue to the same peak load at the same temperature. The difference between macrocomposites and minicomposites could be due to the temperature regime; however, in the minicomposite tests the loading cycle was 0.01 Hz, significantly more rapid than the ref. 19 LCF condition. Also, there may be a significant difference in damage accumulation between cyclic loading of woven macrocomposites and unidirectional minicomposites.

Finally, the susceptibility of these materials to significant strength loss upon return to room temperature after the stress/temperature/time conditions of this study is alarming. Similar behavior was observed by Brewer et al.[19]. It is believed that

the dramatic loss of strength at room temperature is due to the instability of the fibers. If more stable stoichiometric SiC fibers are used, e.g. Sylramic*, Hi-Nicalon type-S**, or Tyranno SA***, a carbon layer should not be formed during MI processing which would prohibit the oxidation along the length of the fiber surfaces.

SUMMARY AND CONCLUSIONS

The rupture properties of Hi-Nicalon, BN-interphase, SiC matrix composites tested in this study showed significant loss in load carrying ability compared to the expected load carrying ability of the reinforcing fibers for the same temperatures and rupture times. Oxidation of the BN interphase and the formation of borosilicate oxidation products causes fiber degradation and strong bonding between individual fibers at locations of near fiber-to-fiber contact. BN interphase oxidation is probably enhanced by the carbon layer formed at the Hi-Nicalon™ fiber surface during matrix processing.

The rate of rupture is controlled by the access of the environment to the load-bearing fibers and the stress-condition applied to the load-bearing fibers. At higher stresses, a faster rate for rupture was observed (Regime I). For this case, through-thickness cracks existed in the matrix due to the initial loading condition. Oxidation ingress occurred from around all sides and edges of matrix cracks into the interior of the composite. Embrittled fibers would fail and shed load onto the remaining fibers. When the load applied to the remaining, unoxidized fibers reached a failure criterion load, based on the reduced load-bearing area, the composite failed. The rupture criterion for the fully loaded pulled-out fibers was that determined by Yun and DiCarlo [25] for the average stress-rupture of individual Hi-Nicalon fibers.

At lower stresses, a slower rupture rate was observed. For this case, microcracks existed in the matrix due to the lower stress loading condition. These cracks would be oxidized and the fibers embrittled. As the embrittled fibers fail due to degradation and strong bonding, the microcracks would grow shedding the loads of the embrittled fibers onto pristine regions of composite. The failure criterion of the remaining pulled-out fibers for this regime was the same as the fast-fracture strength of the Hi-Nicalon fibers in as-produced composites.

Even though embrittlement had occurred at lower stresses, the rate was very slow, allowing greater than 100 hour lifetimes for appreciable applied stresses (> 130 MPa). The rate of damage-accumulation controlled the onset of Regime II behavior and it was found that the material with the higher matrix-cracking stresses had better rupture properties.

The retained strength at room temperature of rupture specimens which did not fail at the applied stresses, but were subjected to a long time test (138 hours),

---

* Dow Corning Corporation, Midland MI
** Nippon Carbon, Tokyo, Japan
*** Ube Industries, Ube City, Japan

was about the same as or slightly less than the applied rupture stress at temperature. This was caused by preferential oxidation, in exposed matrix cracks, of the thin interphases separating closely spaced fibers. Oxidation of the interphase at the fiber-to-fiber contact points then occurred down the length of the fibers away from the matrix crack. The fibers fused together at the fiber-to-fiber contact points resulting in brittle failure when tested at room temperature.

Finally, based on the findings of this study, several recommendations can be made to improve this composite system. (1) Use more stable interphases than CVI BN. (2) Enable greater distances between individual fibers that nearly contact one another. (3) Use more stable fibers that do not decompose to produce carbon layers on their surface and (4) Raise the matrix cracking stresses of the material.

ACKNOWLEDGEMENTS

This work was supported by the HITEMP program at NASA Lewis Research Center. We especially thank Dr. James DiCarlo of NASA Lewis Research Center and Professor James Cawley of Case Western Reserve University for many useful discussions on the results of this work.

REFERENCES:

1. F.E. Heredia, J.C. McNulty, F.W. Zok, and A.G. Evans, "Oxidation Embrittlement Probe for Ceramic-Matrix Composites," *J. Am. Ceram. Soc.*, **78** [8] 2097-2100 (1995).
2. H.T. Lin and P.F. Becher, "Stress-Temperature-Lifetime Working Envelope of Nicalon Fiber-Reinforced SiC Matrix Composites in Air," *Composites Part A*, **28A** 935-942 (1997)
3. E. Lara-Curzio, M.K. Ferber, and P.F. Tortorelli, "Interface Oxidation and Stress-Rupture of NicalonTM/SiC CVCCs at Intermediate Temperatures," Key Engineering Materials Vols. 127-131, Trans Tech Publications, Switzerland, pp. 1069-1082 (1997)
4. G.N. Morscher, "Tensile Stress Rupture of SiCf/SiCm Minicomposites with Carbon and Boron Nitride Interphases at Elevated Temperatures in Air," *J. Am. Ceram. Soc.*, **80** [8] 2029-42 (1997)
5. G.N. Morscher, "The Effect of Static and Cyclic Tensile Stress and Temperature on Failure for Precracked Hi-Nicalon/BN/CVD SiC Minicomposites in Air," *Ceram. Eng. Sci. Proc.*, **18** [3] 737-745 (1997)
6. P. Lipetzky, N.S. Stoloff, and G.J. Dvorak, "Atmospheric Effects on High-Temperature Lifetime of Ceramic Composites," *Ceram. Eng. Sci. Proc.*, **18** [4] 355-362 (1997)
7. M.J. Verilli, A.M. Calomino, and D.N. Brewer, "Creep-rupture Behavior of a Nicalon/SiC Composite," Thermal and Mechanical Test Methods and Behavior of Continuous-Fiber Ceramic Composites, ASTM STP 1309, eds. M.G. Jenkins, S.T. Gonczy, E. Lara-Curzio, N.E. Ashbaugh, and L. Zawada, ASTM pp. 158-175 (1997)

8. E. Lara-Curzio, "Stress-Rupture of Nicalon/SiC Continuous Fiber Ceramic Matrix Composites in Air at 950oC," *J. Am. Ceram. Soc.*, **80** [12] 3268-72 (1997)
9. H.T. Lin and P.F. Becher, Mater. Sci. Eng.
10. T.E. Steyer and F.W. Zok, "Stress Rupture of an Enhanced Nicalon™/SiC Composite at Intermediate Temperatures," *J. Am. Ceram. Soc.* in press.
11. L. Filipuzzi and R. Naslain, "Oxidation Mechanisms and Kinetics of 1D-SiC/C/SiC Composite Materials: I, An Experimental Approach," *J. Am. Ceram. Soc.*, **77** [2] 459-66 (1994)
12. A.J. Eckel, J.D. Cawley, and T.A. Parthasarathy, "Oxidation Kinetics of a Continuous Carbon Phase in a Nonreactive Matrix," *J. Am. Ceram. Soc.*, **78** [4] 972-80 (1995)
13. J.D. Cawley, "Effect of Interphase Carbon Thickness on Environmental resistance of Continuous Fiber-Reinforced Ceramic Matrix Composites," High Temperature Ceramic-Matrix Composites II: Manufacturing and Materials Developoment, Ceramic Transactions V. 58, eds. A.G. Evans and R. Naslain, pp. 377-384 (1995)
14. A.G. Evans, F.W. Zok, R.M. McMeeking, and Z.Z. Du, "Models of High-Temperature, Environmentally Assisted Embrittlement in Ceramic-Matrix Composites," *J. Am. Ceram. Soc.*, **79** [9] 2345-52 (1996)
15. G.N. Morscher, D. Bryant, and R.E. Tressler, "Environmental Durability of BN-Based Interphases (For SiC_f/SiC_m Composites) in H_2O Containing Atmospheres at Intermediate Temperatures," *Ceram. Eng. Sci. Proc.*, **18** [3] 525-533 (1997)
16. N.S. Jacobson, G.N. Morscher, D.R. Bryant, and R.E. Tressler, "High Temperature Oxidation of Boron Nitride Part II: BN Layers in Composites," *J. Am. Ceram. Soc.*, in print
17. W. H. Glime and J.D. Cawley, "Stress Concentration due ot Fiber-Matrix Fusion in Ceramic-Matrix Composites," *J. Am. Ceram. Soc.* **81** [10] 2597-604 (1998)
18. G.N. Morscher and J.Z. Gyekenesi, "Room Temperature Tensile Behavior and Damage accumulation of Hi-Nicalon Reinforced SiC Matrix Composites," *Ceram. Eng. Sci. Proc.*, **19**[3]241-249 (1998)
19. D. Brewer, A. Calomino, and M. Verilli, unpublished research
20. G.N. Morscher, "Modal Acoustic Emission of Damage Accumulation in Woven SiC/SiC at Elevated Temperatures", submitted to Review of Progress in Quantitative Nondestructive Evaluation, Vol. 18, eds. D.O. Thompson and D.E. Chimenti (1999) in press
21. G.N. Morscher, "Modal Acoustic Emission of Damage Accumulation in a Woven SiC/SiC Composite," *Comp. Sci. Tech.* In press.
22. G.N. Morscher, PhD Thesis
23. J.J. Brennan, United Technologies Research Center, unpublished research.
24. L. Thomas-Ogbuji, "A Pervasive Mode of Oxidative Degradation in a SiC-SiC Composite," *J. Am. Ceram. Soc.*, 8 [11] 2777-84 (1998)
25. H.M. Yun and J.A. DiCarlo, "Time/Temperature Dependent Tensile Strength of SiC and Al_2O_3-Based Fibers," Ceramic Transactions Vol 74, Advances in

Ceramic-Matrix Composites III, eds. N.P. Bansal and J.P. Singh. pp. 17-26 (1996)
26. M. Ibnabdeljalil and W.A. Curtin, "Strength and Reliability of Fiber-Reinforced Composites: Localized Load-Sharing and Associated Size Effects," Int. J. Solids Structures, **34** [21] 2649-2668 (1997)
27. Joseph Halada, Allied Signal Corporation, private communication,

Table I: Composite constituent properties

Constituent	Material	Volume Fraction	Elastic Modulus GPa	Details
Fiber	Hi-Nicalon[a]	0.34	280	5 Harness Satin
Interphase	Boron Nitride	0.10	?	~ 0.5 μm thick
Matrix	CVI[b] SiC	0.18	425	~ 2 mm thickness
	&			
	MI SiC + Si	0.34	345	Process Temp. ~ 1400°C
	Porosity	0.04		

[a] Nippon Carbon, Tokyo, Japan; [b] Chemical Vapor Deposition Process

Table II: Fiber grouping from different bundles of an as-produced composite

	Number of fibers (fraction of fibers) In a Given Group of Fibers		
	Surface Ply	***2nd Ply In***	***4th Ply In***
no-touch	24(.048)	22(.044)	22(.044)
in pairs	16(.032)	18(.036)	16(.032)
in triples	9(.018)	9(.018)	9(.018)
in groups < 10	103(.206)	84(.168)	68(.136)
in groups < 20	172(.344)	123(.26)	100(.2)

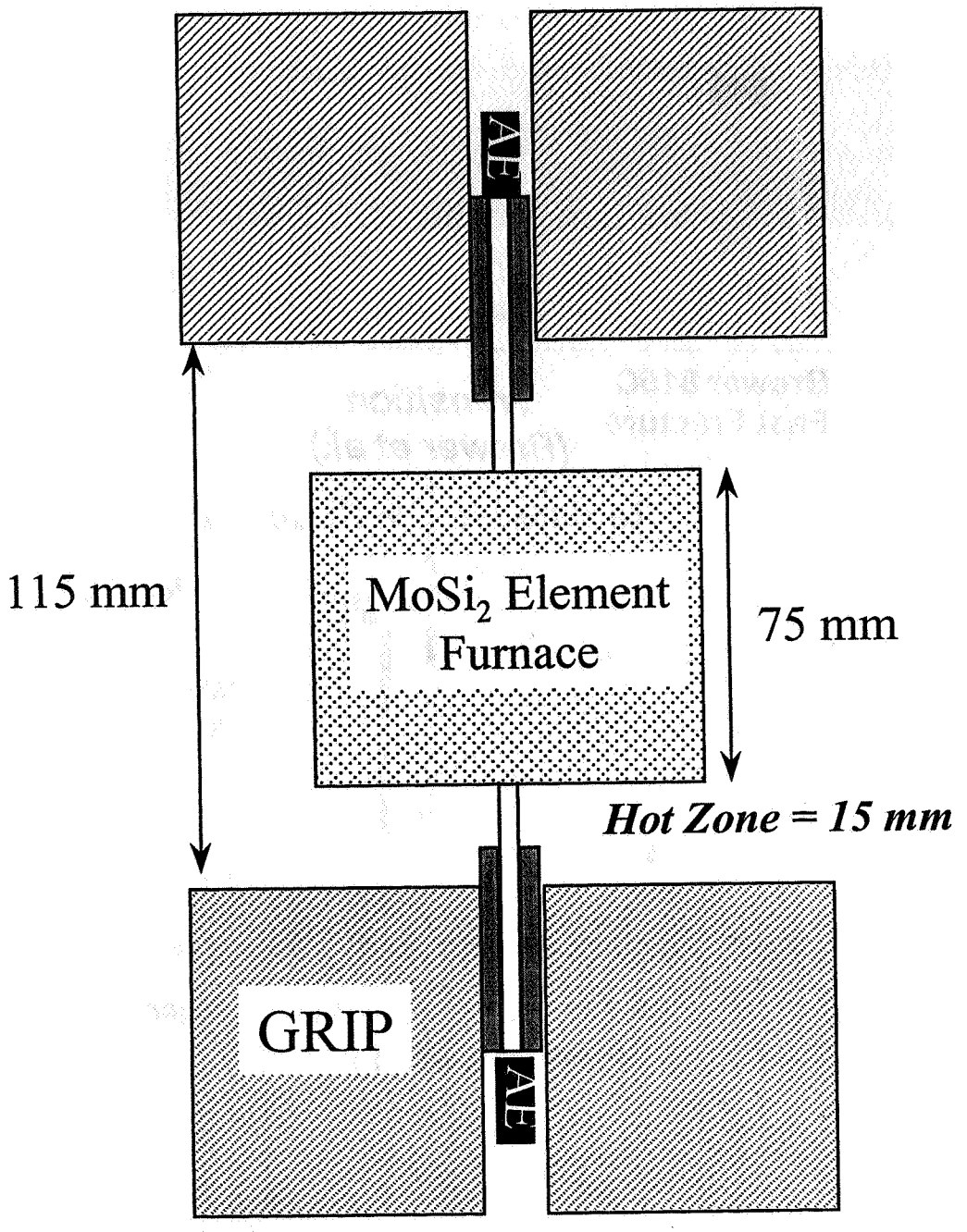

Figure 1: Schematic representation of tensile rupture test set up.

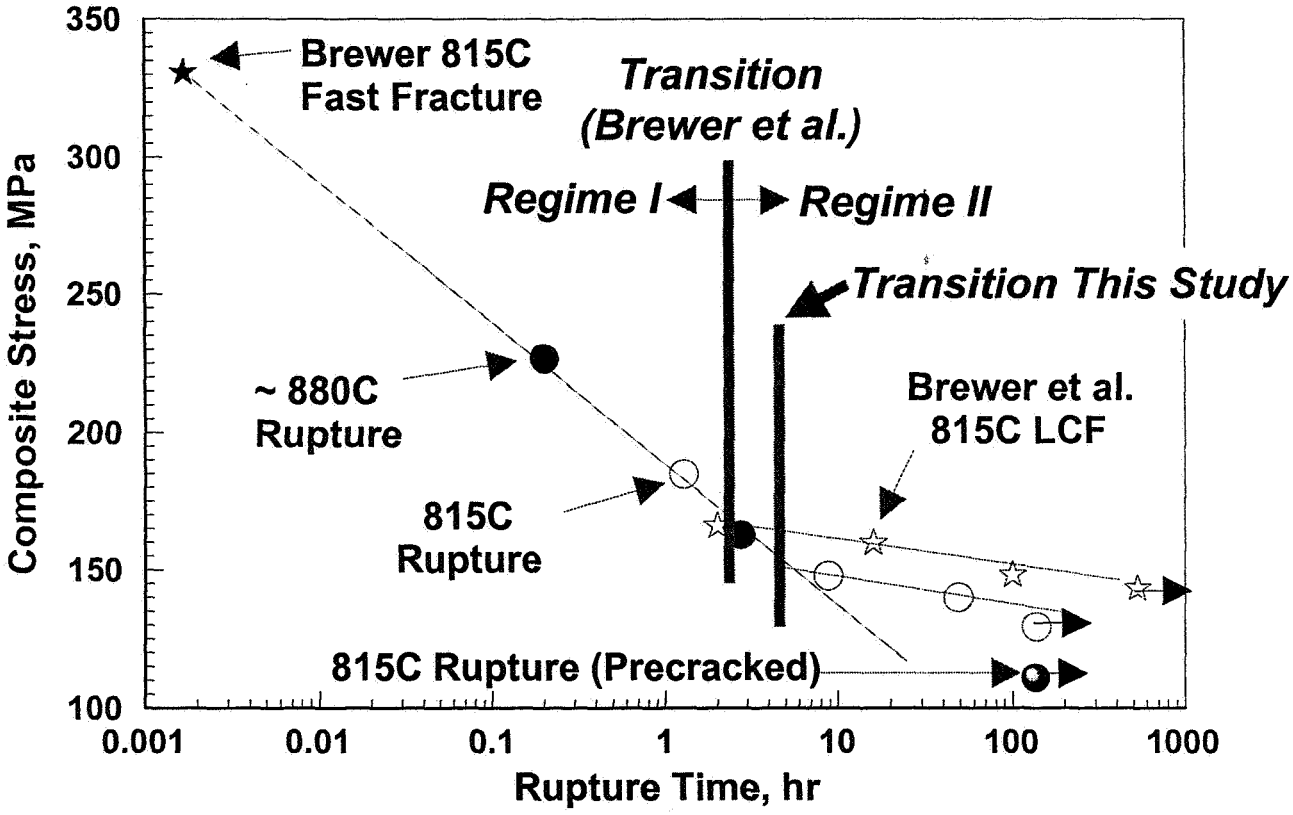

Figure 2: Stress-rupture data from this study and LCF data from ref. 19 plotted verses time. Also plotted is the 815°C fast fracture strength of the material tested in ref. 19.

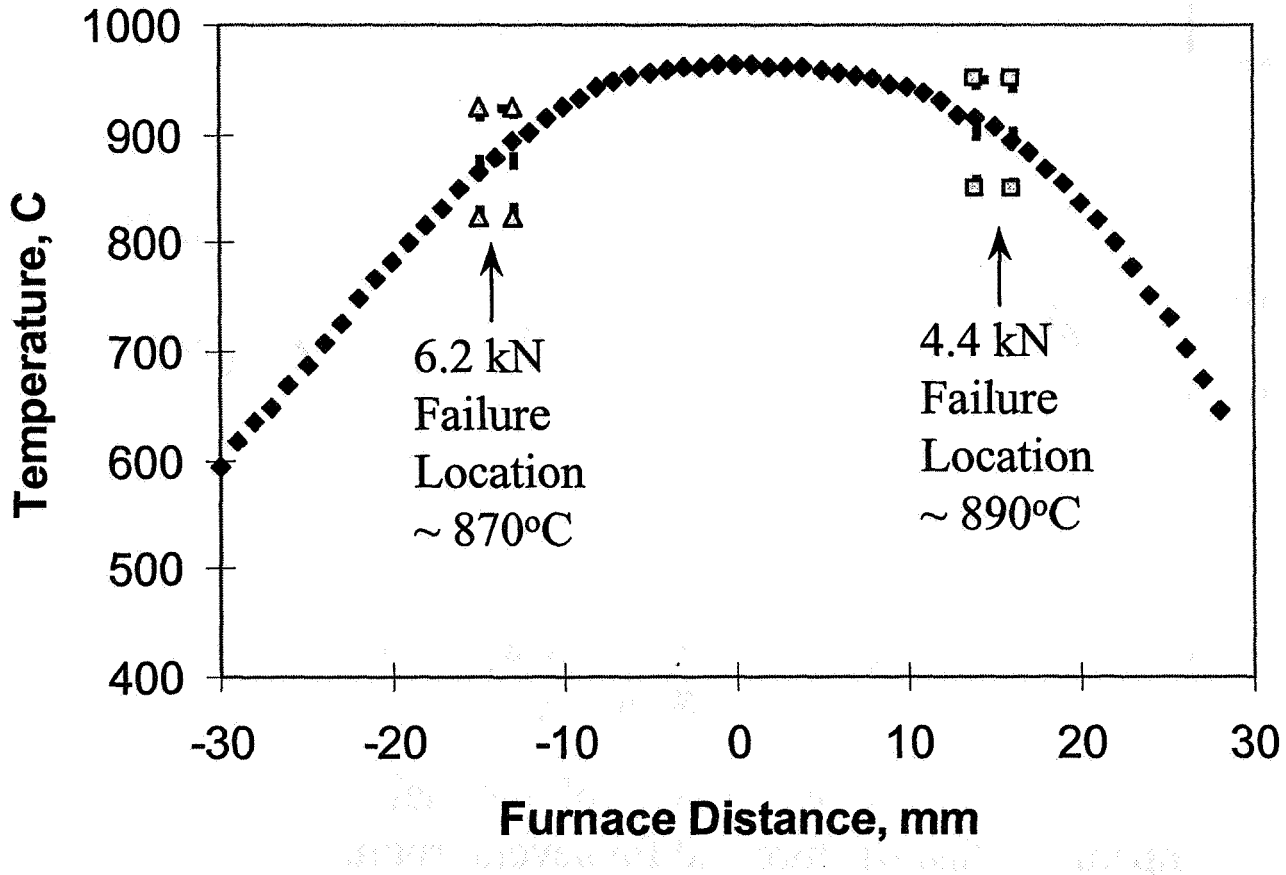

Figure 3: Furnace profile and location of failure for first two stress-rupture experiments.

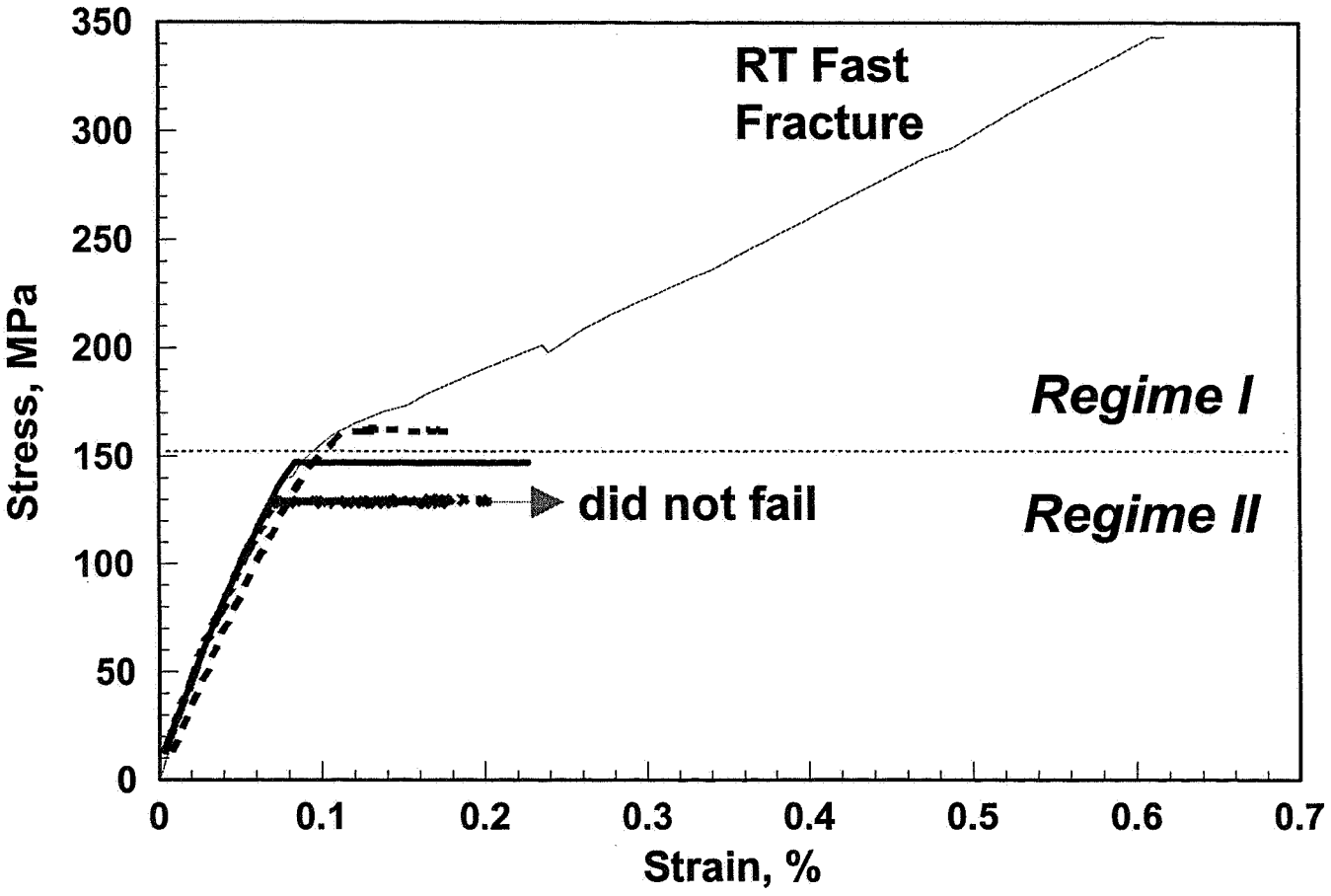

Figure 4: Stress-strain behavior of material tested at room temperature fast fracture and for several rupture tests. Note that the apparent load drops in the RT fast fracture curve are actually associated with unload/reload hysteresis loops which have been removed from the stress-strain curve for clarity. Also, the failure location of the RT fast fracture specimen occurred in the grips; therefore, the ultimate strength is greater than the failure stress shown in this figure.

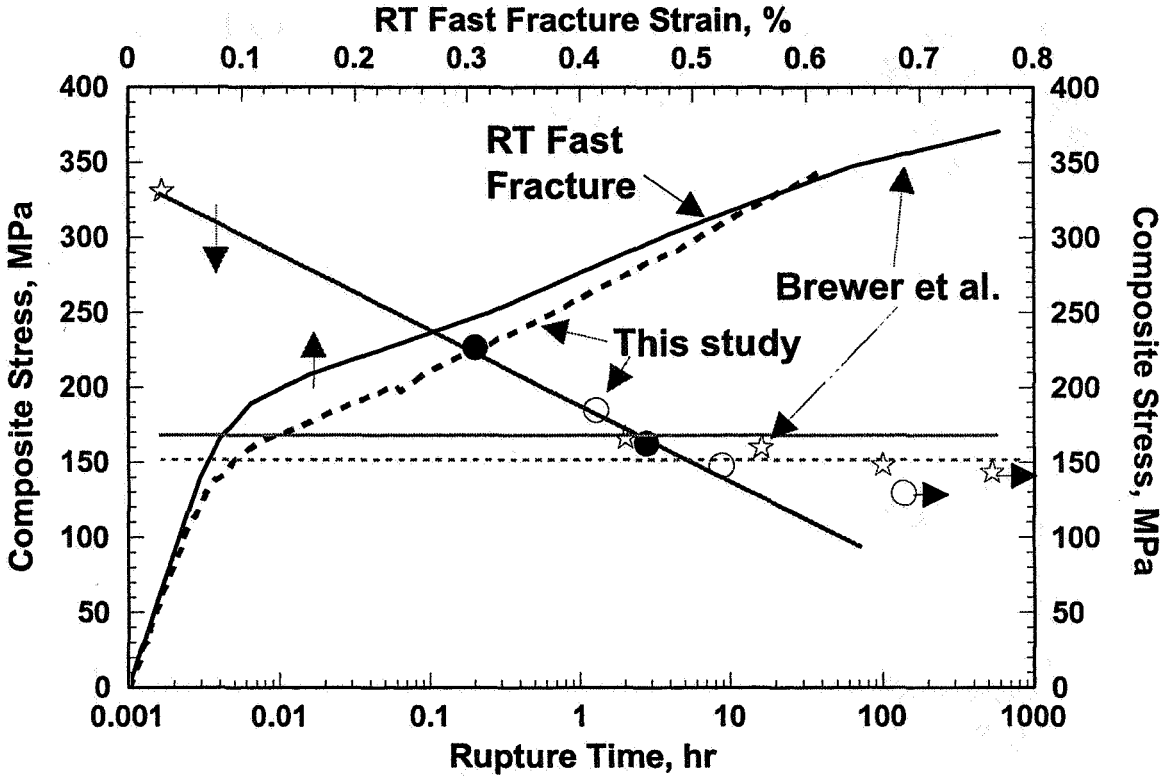

Figure 5: Room temperature and time dependent stress-rupture behavior of the two different Hi-Nicalon, BN interphase, MI SiC composites (data points the same as for Figure 2). The horizontal line corresponds to the transition stress for Regime I and Regime II rupture behavior for the two composites. For both samples tested at room temperature, failure occurred in the grips and not in the gage section. There is actually little difference in the ultimate properties of these two composites.

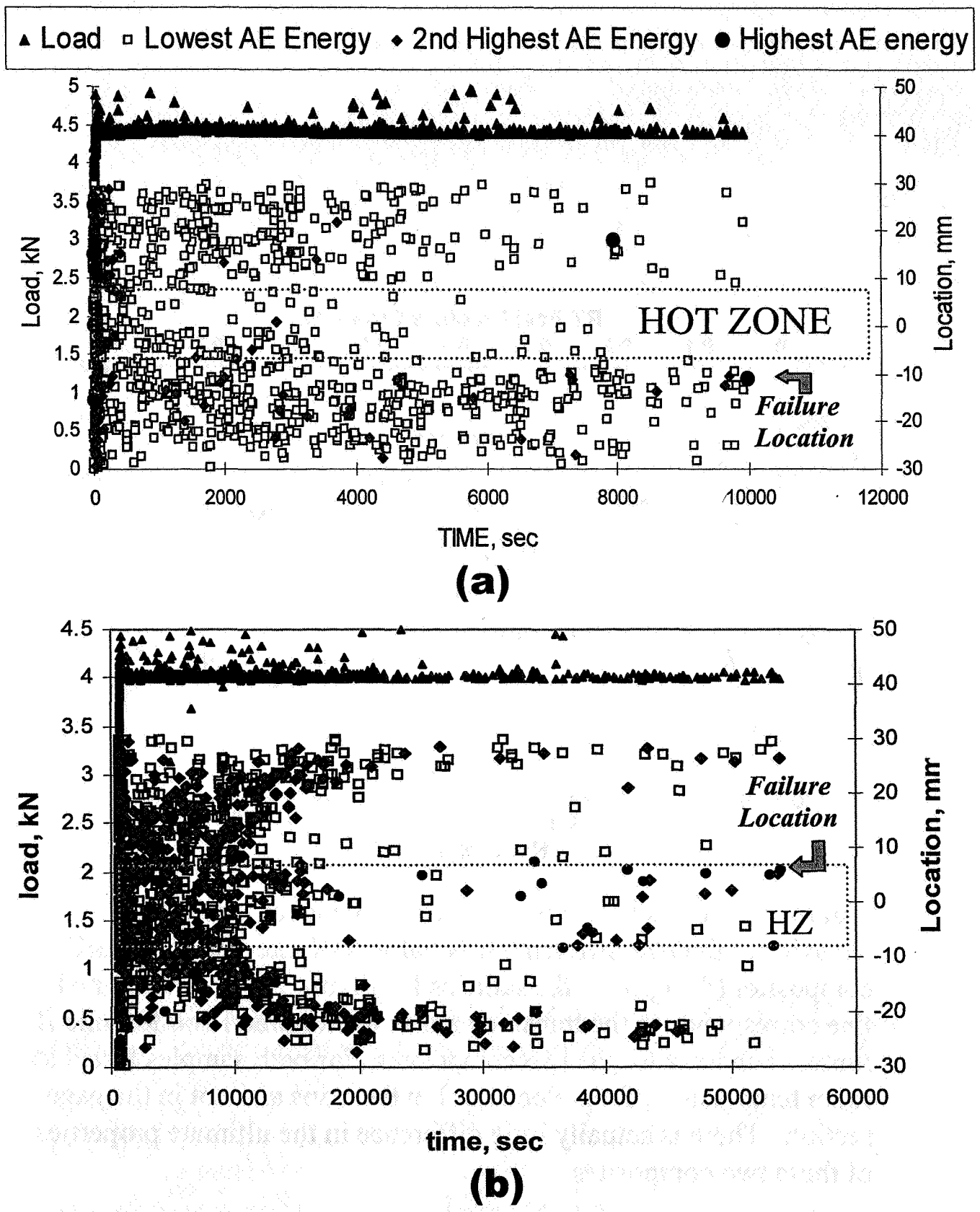

Figure 6: Load and AE event location versus time for (a) an applied load of 4.4 kN (160 MPa) at 960°C hot zone temperature and (b) an applied load of 4 kN (148 MPa) at 815°C hot zone temperature.

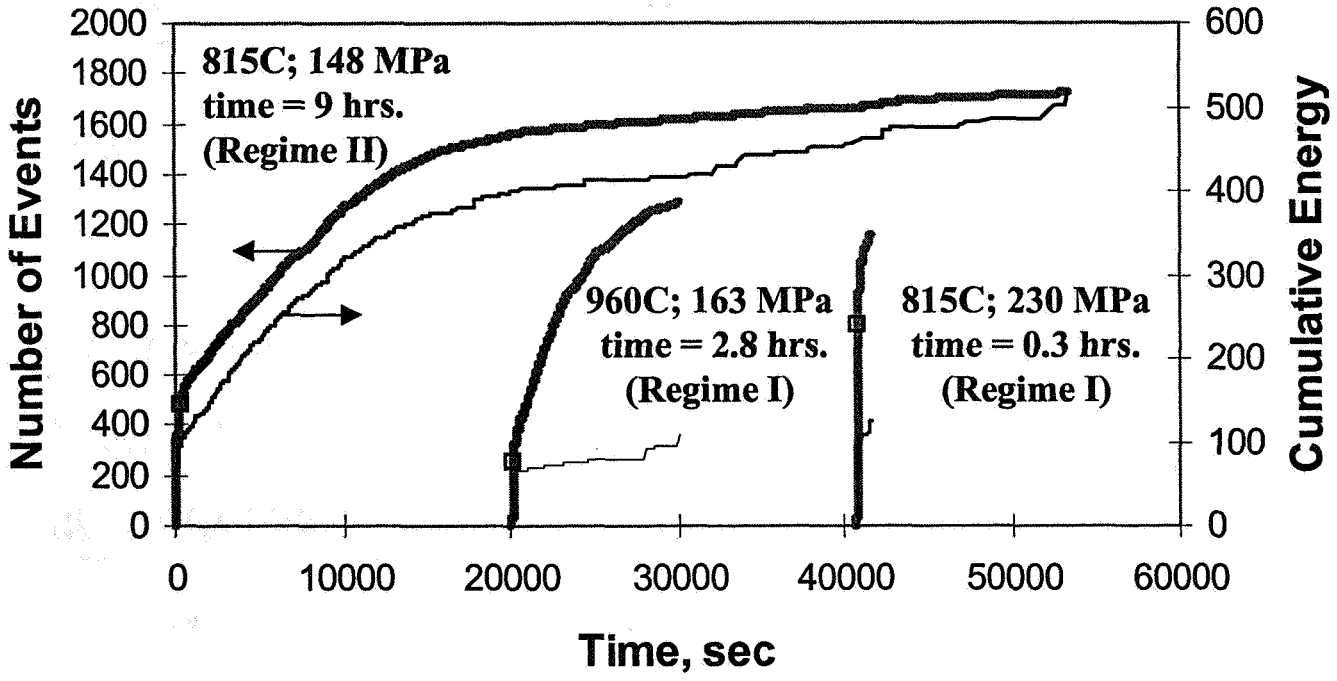

Figure 7: The cumulative number of AE events and cumulative AE energy as a function of time for three rupture specimens. The square on the "number of events" curves indicates the time at which the load reached the set-load for the rupture experiment. The two shorter time experiment data sets are offset on the time scale for clarity.

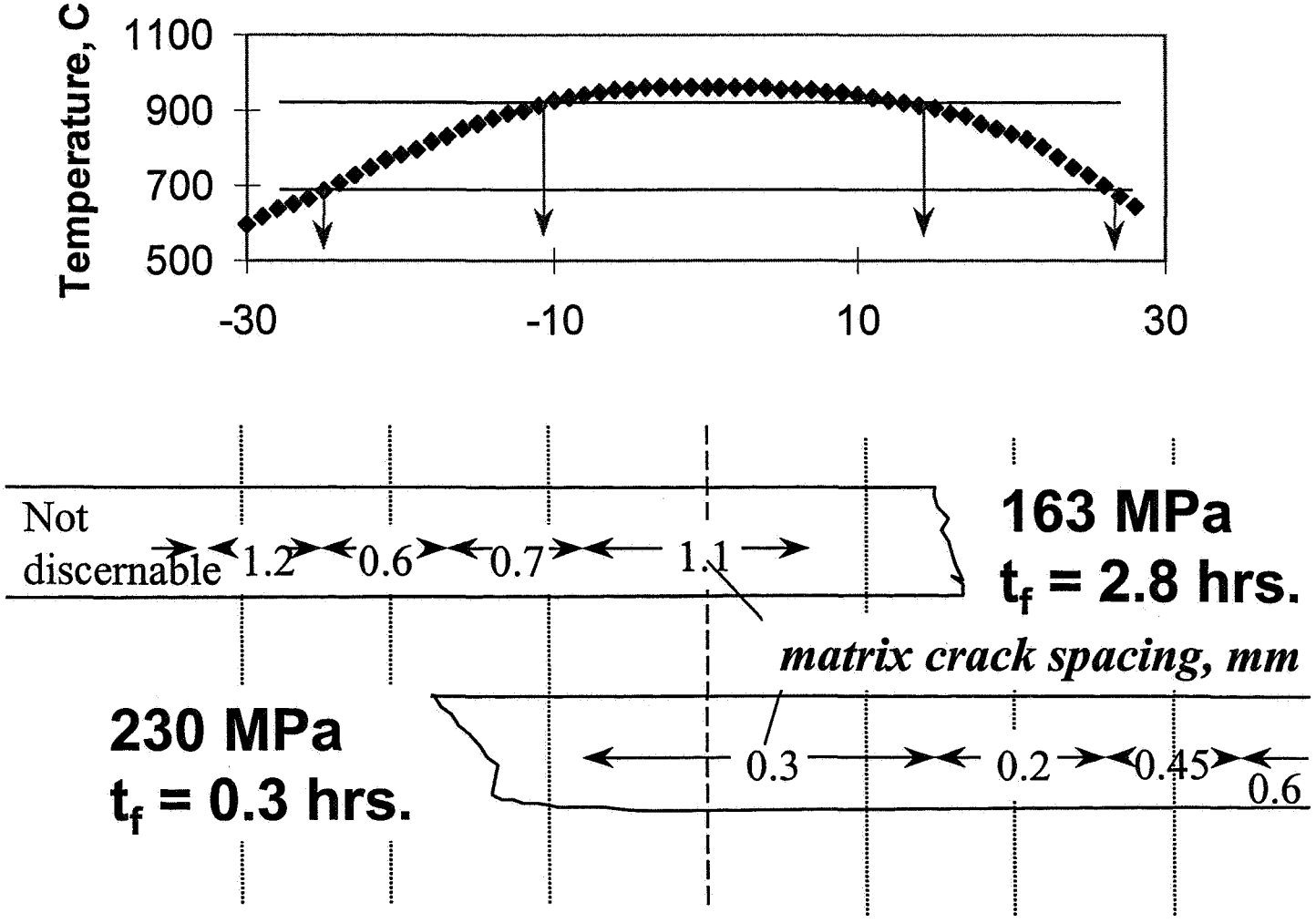

Figure 8: Measured matrix cracking for two samples tested at 960°C over the length of each sample as well as the furnace temperature profile (Figure 3) as a function of length.

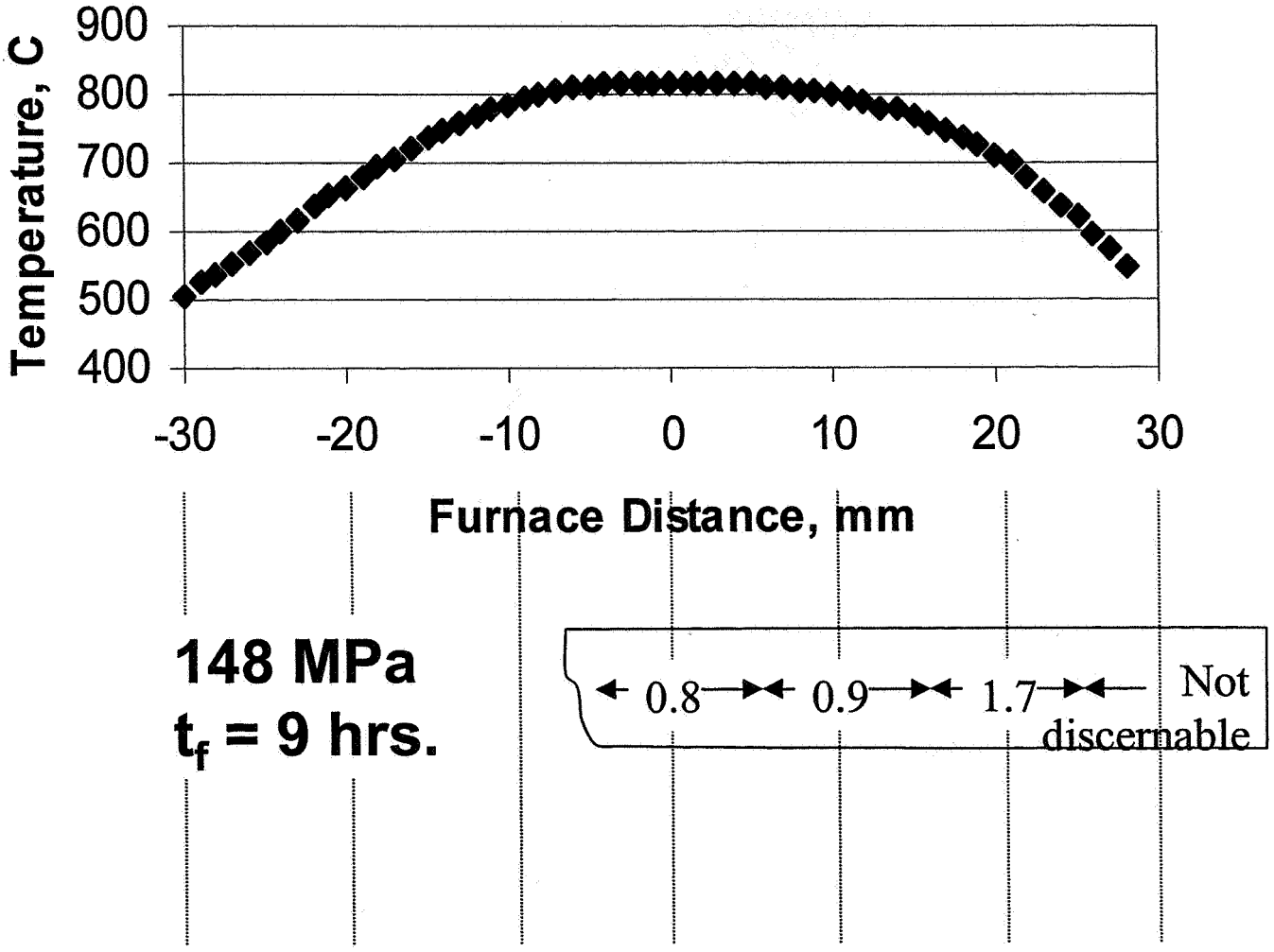

Figure 9: Measured matrix cracking for a sample tested at 815°C over the length of the sample as well as the furnace temperature profile as a function of length.

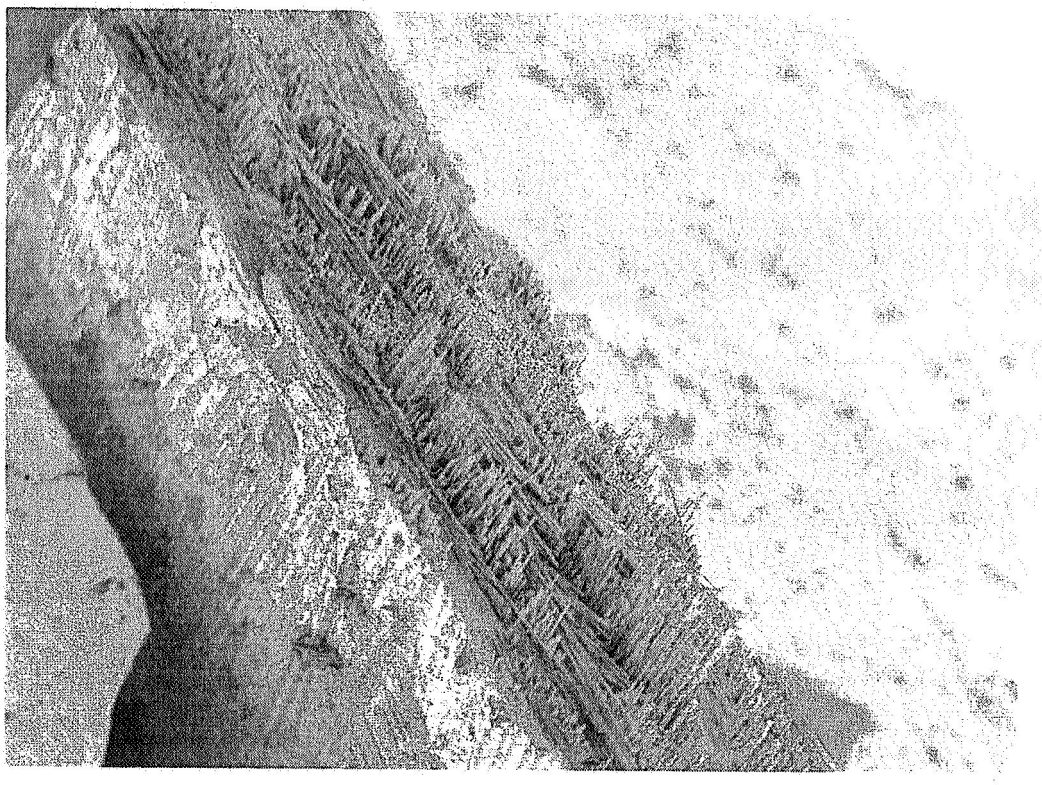

(a)

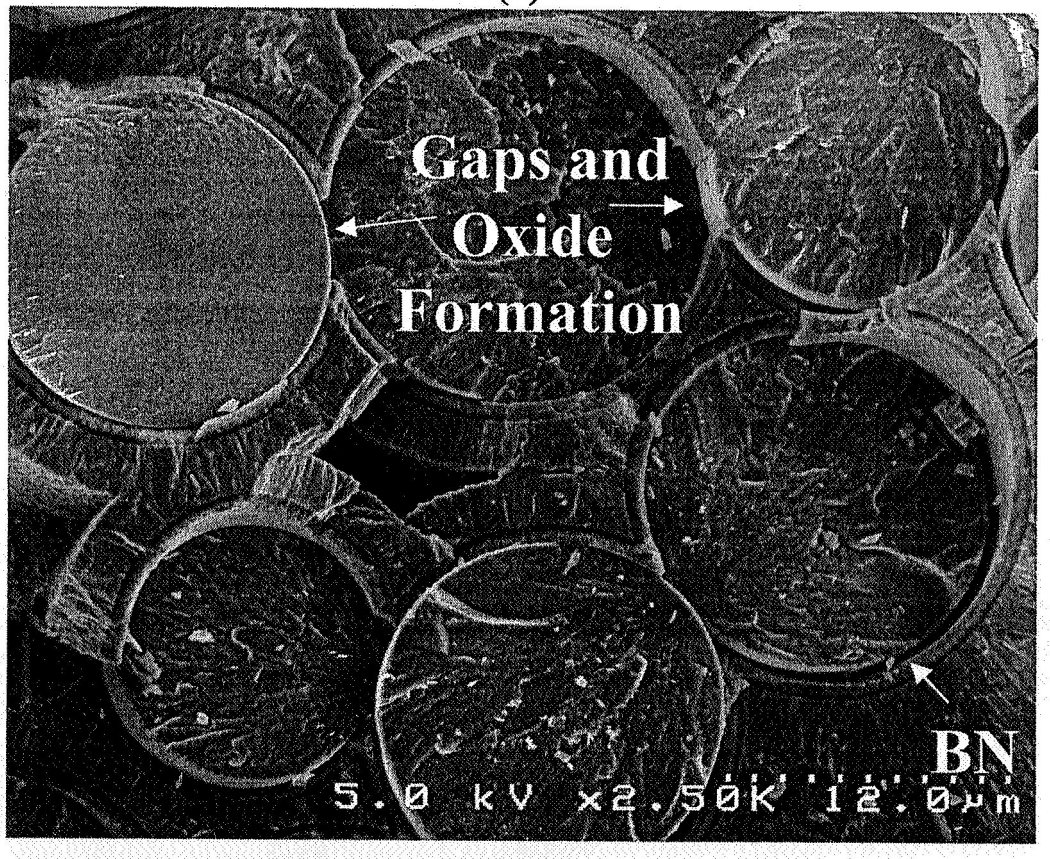

(b)

Figure 10: (a) Fracture surface of Regime I specimen tested at 180 MPa. The rupture time was 1.1 hours. (b) Higher magnification region showing embrittled fibers.

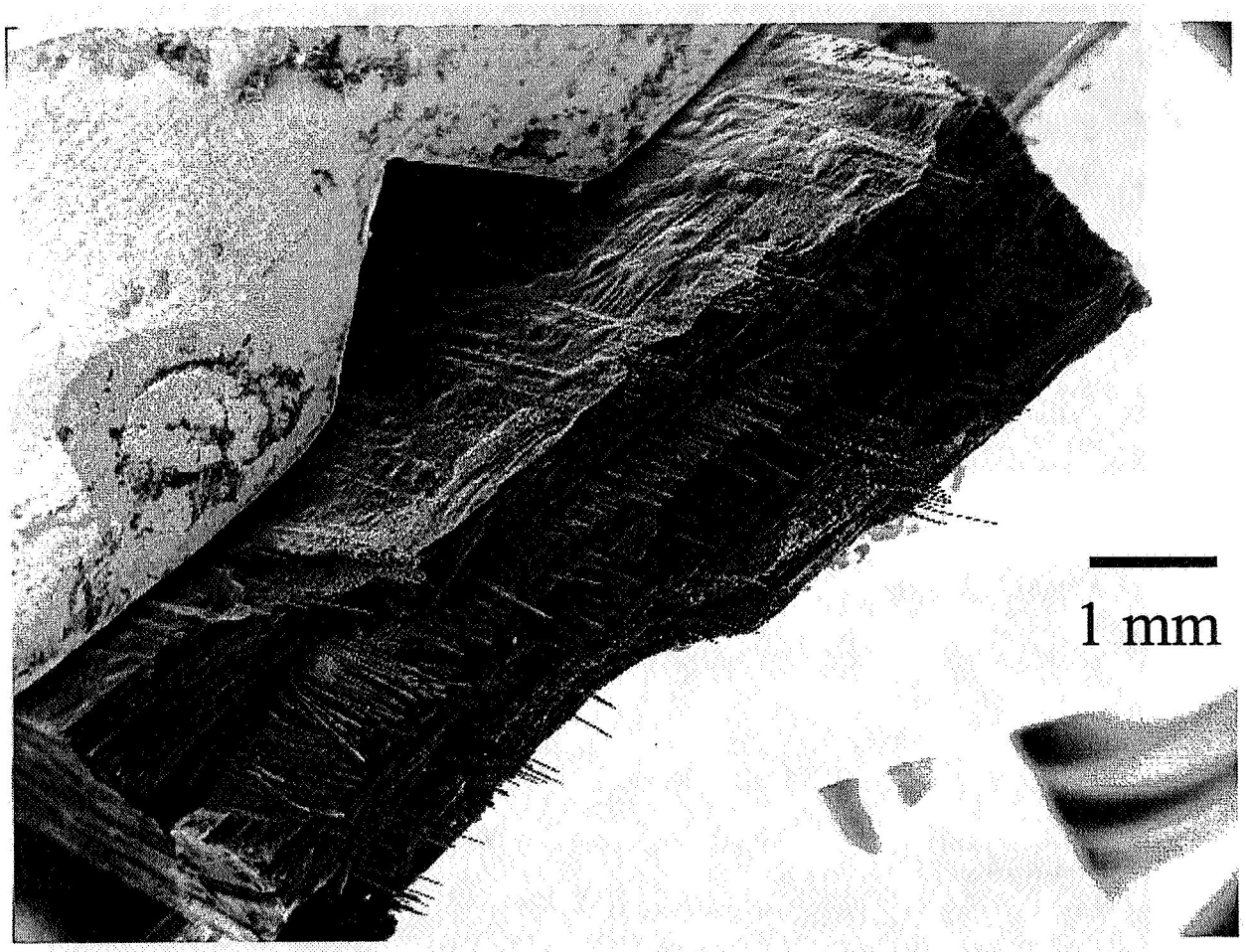

Figure 11: (a) Fracture surface of Regime II rupture failure for fracture surface obtained from ref. 19. The applied stress was 160 MPa and the rupture time was 18.1 hours. (b, c) Higher magnification regions showing the oxidation front and region of pristine fibers.

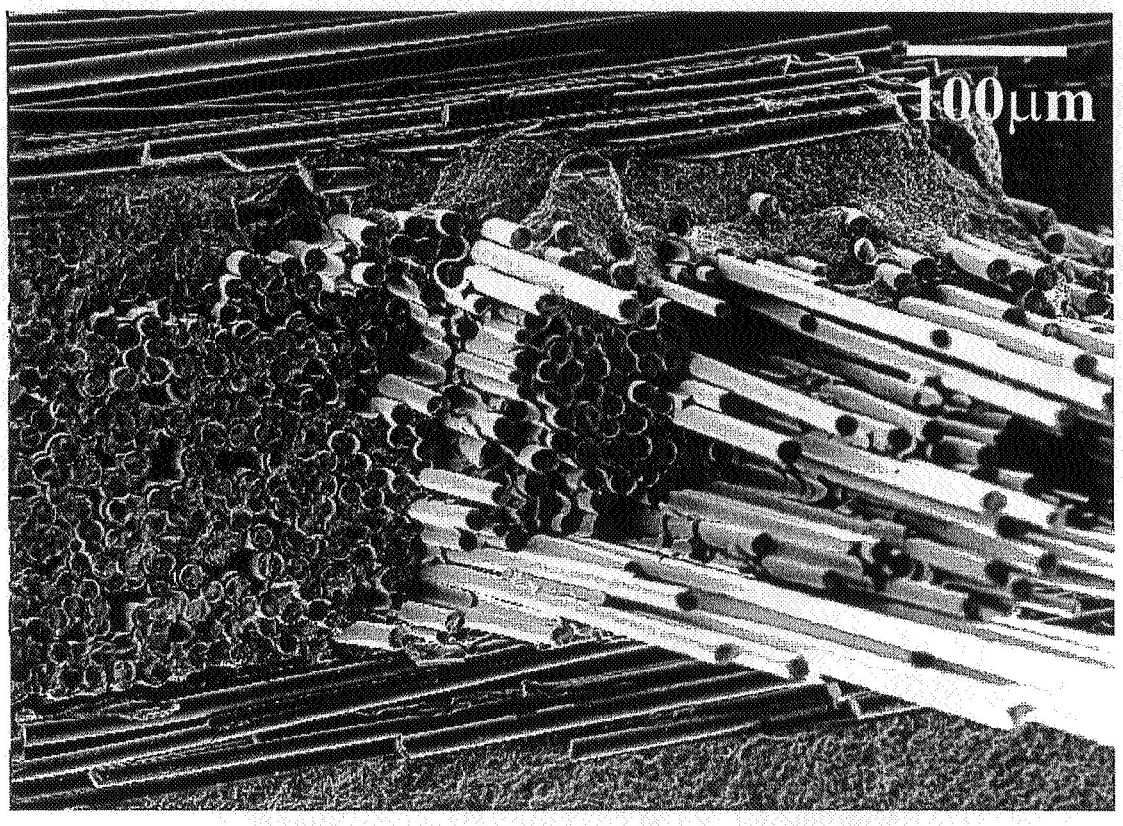

(b)

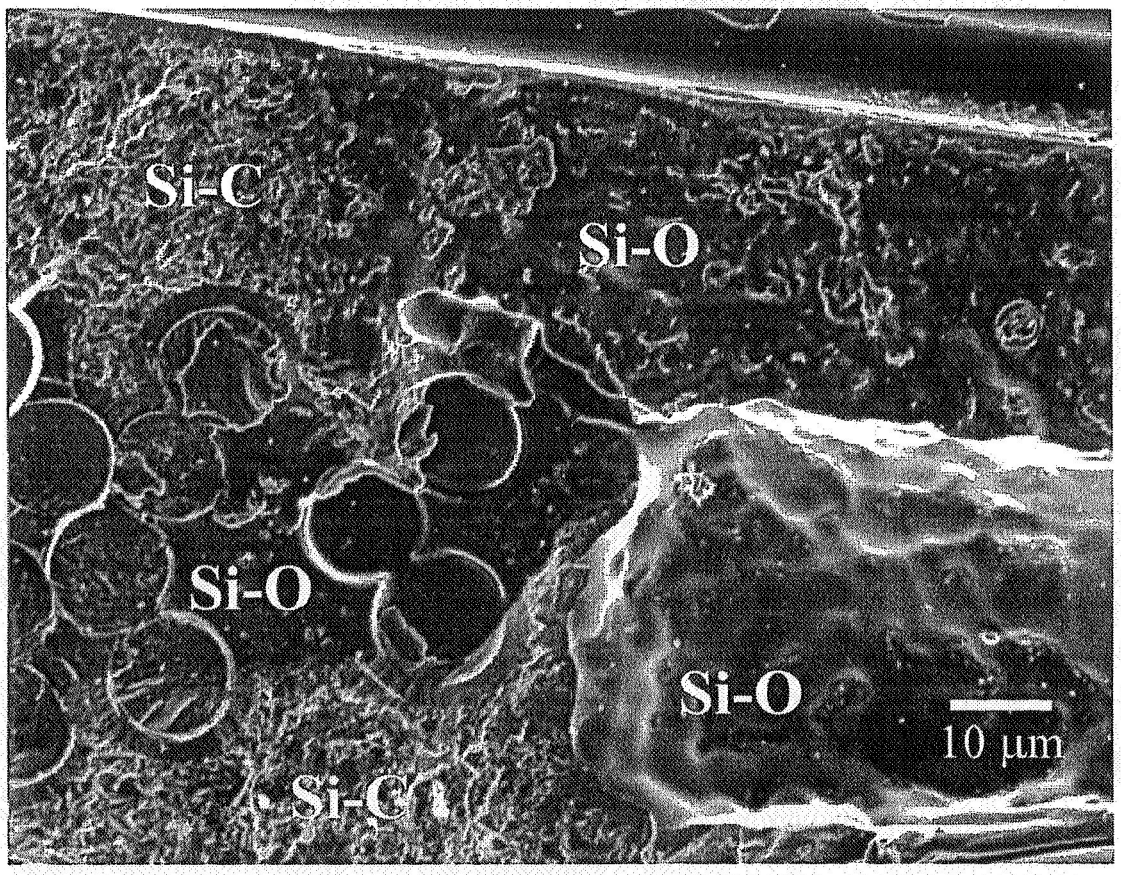

(c)

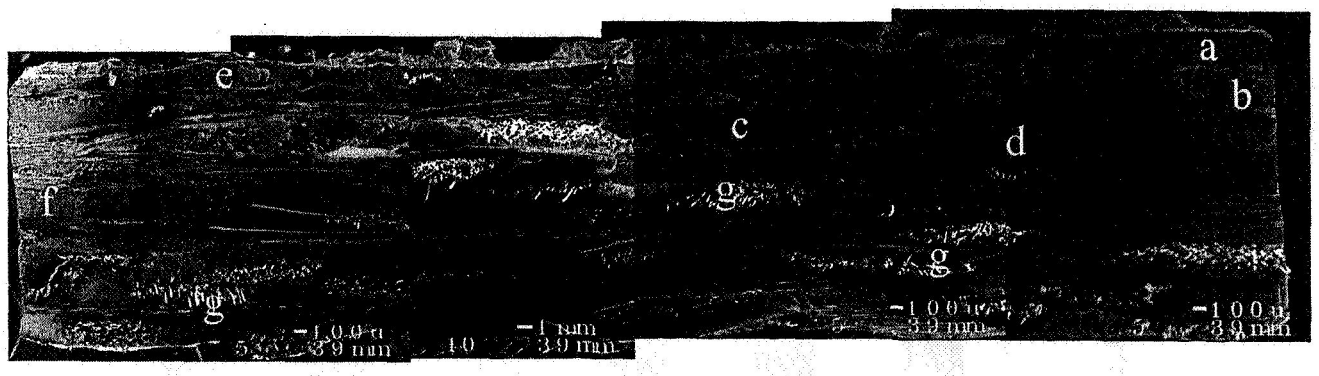

(a)

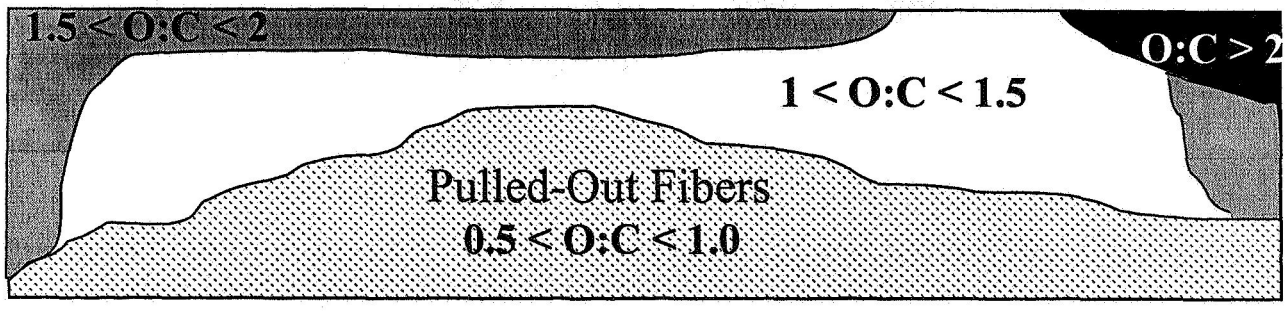

(b)

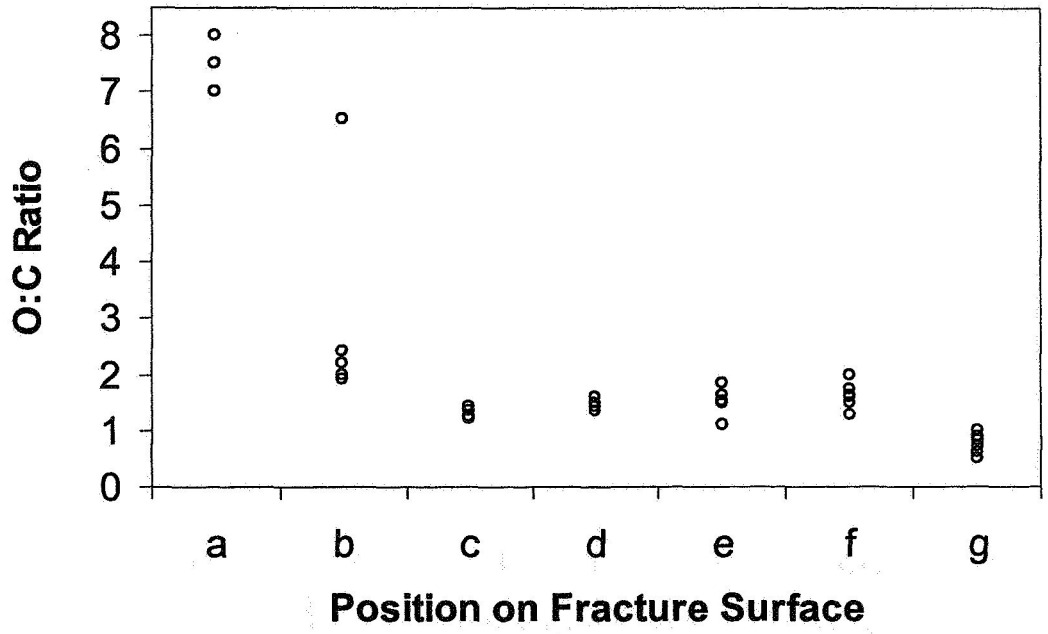

(c)

Figure 12: Fracture surface (a) of a specimen ruptured after 114 hrs and 148 MPa [19]. EDS was performed on individual fiber fracture surfaces and the O:C ratio was measured for 17 different bundles, some of which are shown in (c). A map was constructed based on the O:C ratios (b).

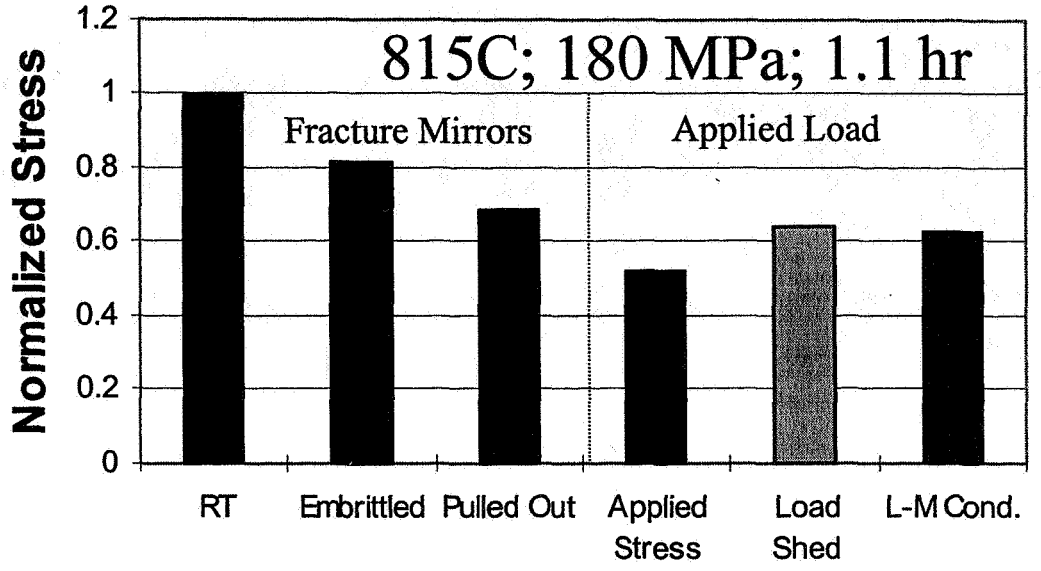

(a)

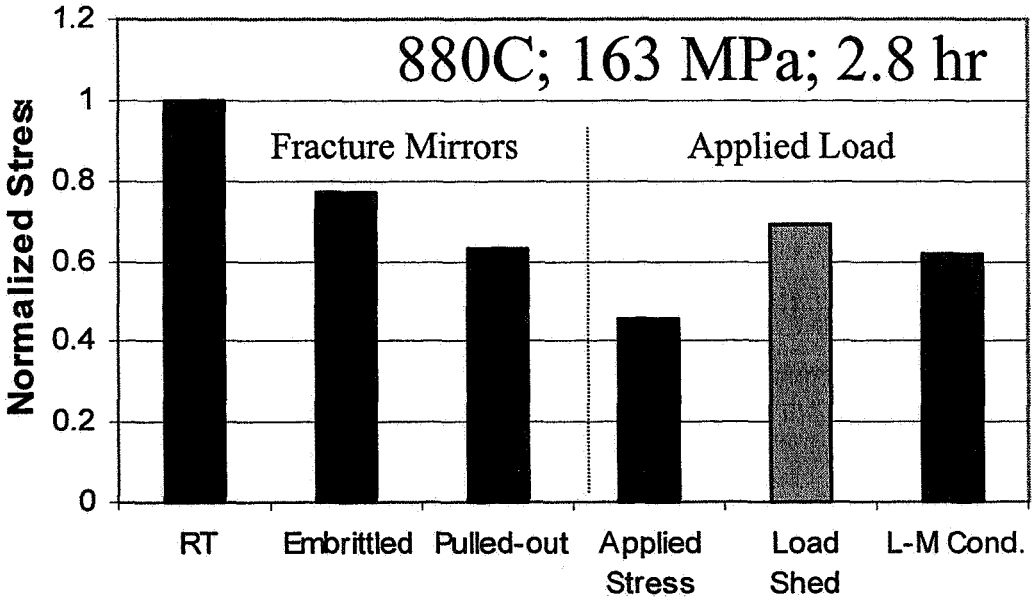

(b)

Figure 13: Bar charts of the normalized stress as determined from the fracture mirror analysis for two Regime I rupture specimens. Also plotted is the normalized applied stress, the normalized stress from the load shed by the embrittled fibers, and the Larson-Miller condition for fiber failure[25].

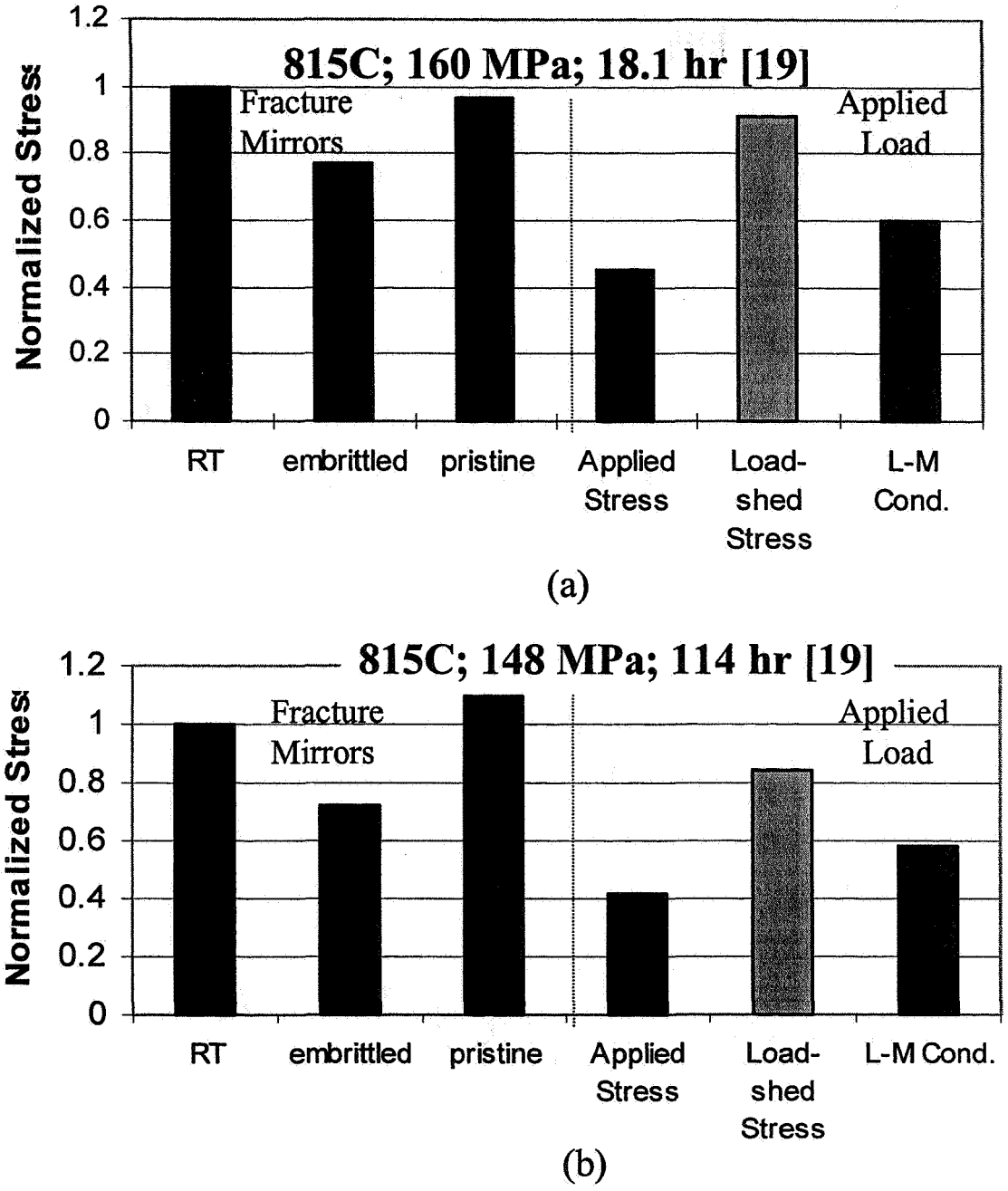

Figure 14: Bar charts of the normalized stress as determined from the fracture mirror analysis for two Regime II rupture specimens. Also plotted is the normalized applied stress, the normalized stress from the load shed by the embrittled fibers, and the Larson-Miller condition for fiber failure[25].

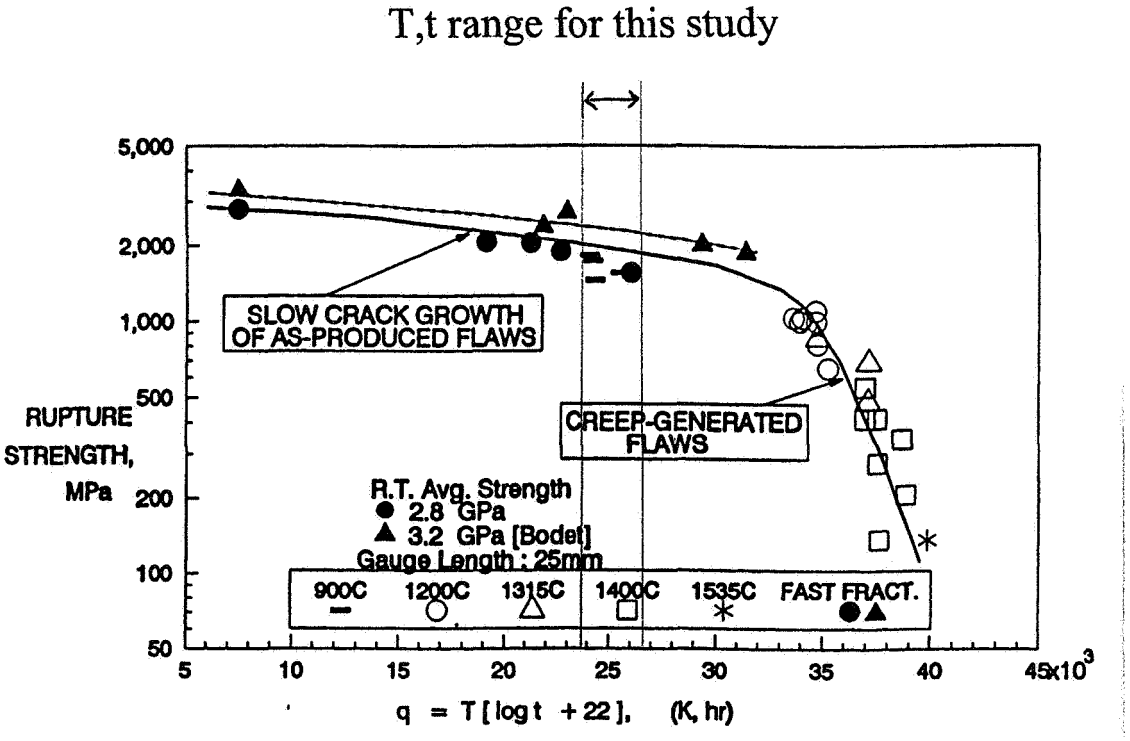

Figure 15: Larson-Miller plot for stress-rupture properties of individual as-produced Hi-Nicalon™ fibers in air [25]. Used with permission.

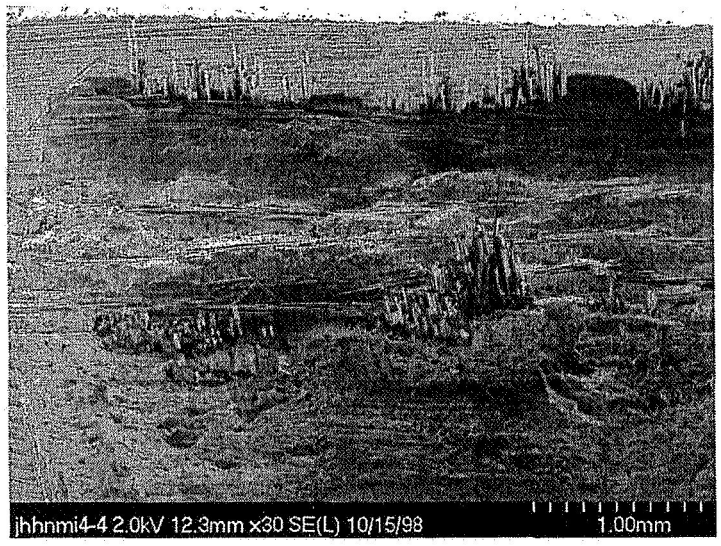

(a)

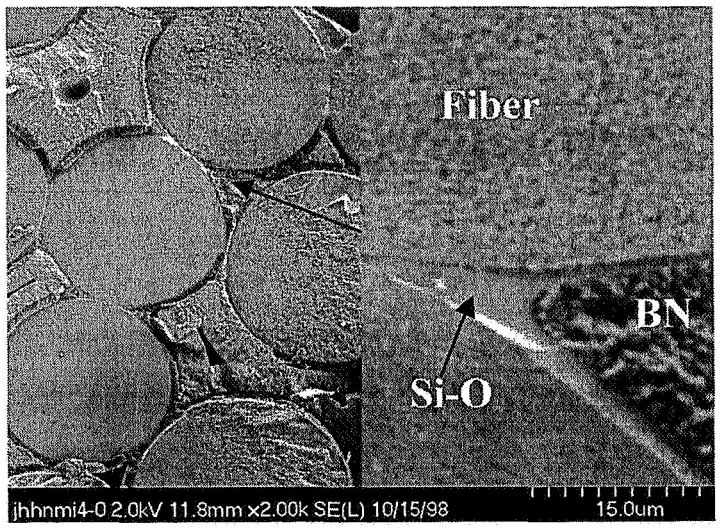

(b)

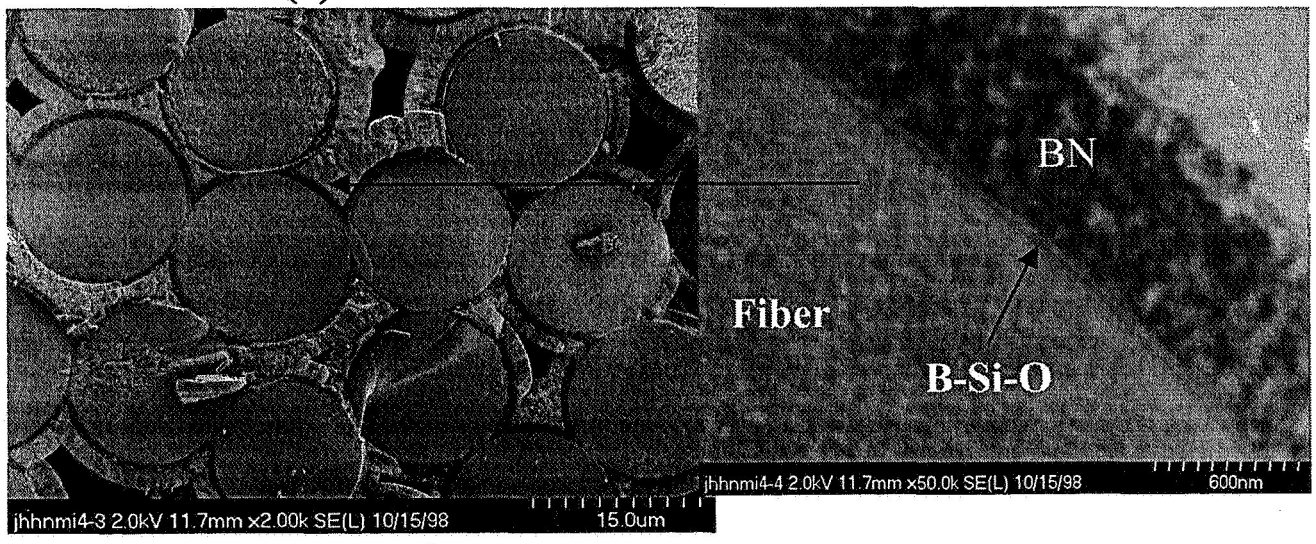

(c)

Figure 16: SEM micrographs of specimen tested at room temperature after 138MPa, 138 hour at 815°C. (a) Some pull-out occurred on some of the outer tows. (b) Most of the bundles showed no pull-out and oxide formation at the near fiber-to-fiber contact regions and in between the BN and the fiber (c).